An ancestral haplotype of P2RX5 yields a B-cell surface marker and a promising multi-lineage immunotherapy target

Zhiwei Ang,[1] Annette Castro,[1] Luca Paruzzo,[2,3,4] Carolin Schimdt,[1] Zainul S. Hasanali,[4] Katharina E. Hayer,[5] Federico Stella,[2,3,4] Samantha S. Soldan,[6] Manuel Torres-Diz,[1] Christopher Kwok,[7] Patricia King Sainos,[8] Kayla Ji, [8] Patrick J Krohl,[9,10] Justyn Fine,[10,11] Priyanka Sehgal,[1] Daniel Martinez,[12] Jamie B. Spangler,[9,10] James L. Riley,[13] Dan T. Vogl,[4] Patrizia Porazzi,[2,3,4] Vinodh Pillai,[14,15] Paul M. Lieberman,[6] David Allman,[14] Marco Ruella,[2,3,4] and Andrei Thomas-Tikhonenko [1,14,16,17,18]

[1] Division of Cancer Pathobiology, Children's Hospital of Philadelphia, Philadelphia, PA
[2] Center for Cellular Immunotherapies, Perelman School of Medicine at the University of Pennsylvania, Philadelphia, PA
[3] Lymphoma Program, Abramson Cancer Center, University of Pennsylvania, Philadelphia, PA;
[4] Division of Hematology/Oncology, Perelman School of Medicine at the University of Pennsylvania, Philadelphia, PA
[5] Department of Biomedical and Health Informatics, Children's Hospital of Philadelphia, Philadelphia, PA
[6] Genome Regulation and Cell Signaling Program, The Wistar Institute, Philadelphia, PA
[7] Vagelos Life Sciences Management Program, University of Pennsylvania, Philadelphia, PA, USA
[8] Department of Biology, College of Arts and Sciences, University of Pennsylvania, Philadelphia, PA
[9] Department of Chemical & Biomolecular Engineering, Johns Hopkins University School of Engineering, Baltimore, MD, USA.
[10] Department of Biomedical Engineering and Translational Tissue Engineering Center, Johns Hopkins University School of Medicine, Baltimore, MD, USA.
[11] Program in Molecular Biophysics, Johns Hopkins University, Baltimore, MD 21208, USA
[12] Pathology Core, Children's Hospital of Philadelphia, Philadelphia, PA
[13] Department of Microbiology, Perelman School of Medicine at the University of Pennsylvania, Philadelphia, PA
[14] Department of Pathology and Laboratory Medicine, Perelman School of Medicine at the University of Pennsylvania, Philadelphia, PA
[15] Division of Hematopathology, Children's Hospital of Philadelphia, Philadelphia, PA
[16] Senior author
[17] Twitter: @andrei_thomas_t
[18] Lead contact
*Correspondence: andreit@pennmedicine.upenn.edu

SUMMARY

Immunotherapies targeting B-cell and plasma lineage markers (e.g., CD19 and BCMA) have improved outcomes for B-cell leukemias/lymphomas (B-ALL/BCL) and multiple myelomas (MM) patients. However, antigen-negative/low relapses are common, and few alternative targets exist. Furthermore, the use of lineage markers in T-cell leukemia (T-ALL) is problematic, as it causes CAR T-cell fratricide. Here, using transcriptomic datasets and newly-developed anti-P2RX5 monoclonal antibodies (mAbs), we show that *P2RX5* mRNA expression is B-cell lineage-restricted in healthy individuals, but is sustained/reactivated in BCL, T-ALL, and MM. Furthermore, due to the favorable haplotype, >80% of people of African descent express a stable, plasma membrane-bound P2RX5 protein. To credential it as a multi-lineage therapeutic target, we reformatted P2RX5-directed mAbs into bispecific T-cell engagers and CAR T-cells. These immunotherapeutics exhibited high potency in cell culture and xenograft models of BCL, T-ALL, and MM, comparable to CD19-directed blinatumomab and BCMA-directed ciltacabtagene autoleucel and active against CD19- and BCMA-negative variants.

KEYWORDS

Purinergic receptors, RNA splicing, B cell development, hematologic malignancies, cellular immunotherapies

INTRODUCTION

Immunotherapies targeting B-lymphoid lineage markers (e.g., CD19, CD20, CD22, and BCMA) have gained wide acceptance in the clinic for the treatment of B-lymphoid and plasma cell malignancies, due to their proven safety and efficacy. A prime example is CD20, which almost 30 years ago became the first clinically developed immunotherapy target [1] . To date, half a dozen anti-CD20 mAbs (with rituximab as the prototype [1,2]) and three anti-CD20xCD3 bispecifics (mosunetuzumab [3], epcoritamab [3], and glofitamab [4]) have gained FDA approvals for the treatment of B-cell lymphoma (BCL).

Because most precursor B-cell acute lymphoblastic leukemias (B-ALL) do not express CD20, these patients are routinely treated with blinatumomab, a CD19-CD3 bi-specific T-cell engager (BiTE) [5], for relapse/refractory (r/r) disease and, more recently, in the frontline setting (the consolidation phase) [6]. Additionally, for the past 10 years, various iterations of CD19-directed chimeric antigen receptor (CAR)-armed T cell products (CART-19: tisagenlecleucel [7], axicabtagene ciloleucel [8], and lisocabtagene maraleucel [9]) have been in clinical use for both B-ALL and BCL.

Despite high initial response rates, up to half of patients with B-ALL or BCL will relapse after CART-19 treatment [10,11], primarily due to CD19 loss [12-17]. Patients with CD19-negative B-ALL relapses are usually treated with some form of salvage immunotherapy directed against CD22 [18]. These also come in two main modalities: the antibody-drug conjugate (ADC) inotuzumab ozogamycin (InO), which has been in wide clinical use for almost 8 years [19-21], and autologous CAR T cells (CART-22) currently undergoing clinical trials [22,23]. Although these salvage immunotherapies can be quite effective, CD22 downregulation has been observed following immunotherapy with both CART-22 and InO, in both children and adults, and in both B-ALL and BCL patients [23-29]. Once CD22 loss has occurred, no 'third-line' immunotherapy options are readily available.

The scarcity of validated targets is especially acute in the case of multiple myeloma (MM), the malignant cancer of plasma cells, which despite their B-cell origin, express little to no CD20, CD19, or CD22. Consequently, immunotherapies for MM are directed against a different set of surface protein, most frequently B-cell maturation antigen (BCMA) [30] and G-protein coupled receptor family C group 5 member D (GPRC5D) [31]. In fact, two anti-BCMA CARs (ciltacabtagene autoleucel [32] and idecabtagene vicleucel [33]) as well as anti-BCMA and anti-GPRC5D bispecific T-cell engagers (teclistamab 35661166 [34] and talquetamab 36507686 [35]) are currently in clinical use in the relapse setting. However, BCMA-directed immunotherapies are survival-prolonging but not curative, due most frequently to the downregulation of the cognate epitope [36-38]. While new targets for cellular immunotherapies (e.g., SEMA4A [39]) are being developed, these novel approaches are yet to reach the clinic.

In the case of T-cell leukemias and lymphomas, the use of lineage markers (e.g., CD3, CD5 or CD7) to redirect CAR T-cell is further complicated by the fact that it can causes CAR T-cell fratricide and aplasia [reviewed in Ref. [40]]. Thus, the need to discover truly T-ALL/TCL-specific surface antigens could not be more urgent.

Here, we show that the ATP-gated ion channel known as P2X purinoceptor 5, or P2RX5 (reviewed in Ref. [41]), is a promising immunotherapy target for a subset of patients with a broad range of hematologic malignancies. The *P2RX5* gene is robustly transcribed across BCL, T-ALL, and MM samples, while in normal tissues its transcription, much like that of CD19, is restricted to mature B cells. In many human populations, the *P2RX5* gene carries two linked single nucleotide polymorphisms (SNP), rs891746 and rs3215407, adversely affecting pre-mRNA splicing, disrupting its open reading frame, and essentially rendering it a pseudogene. However, almost 80% of individuals of African descent carry the favorable, ancestral haplotype (non-reference allele) yielding a stable, full-length, plasma membrane-bound P2RX5 (P2RX5-FL). Thus, we generated two anti-P2RX5 mAbs, 1D9 and 2F4, and showed that they can be used in flow cytometric assays and immunohistochemical (IHC) assays to correctly identify normal B cells and neoplastic BCL, T-ALL, or MM cells. We then converted 1D9 and 2F4 into P2RX5-CD3 bi-specifics and CARs, which displayed potent cytolytic activity against various P2RX5-FL-positive blood cancer cell lines, including CD19- and BCMA-negative variants. These findings suggest that they could become either frontline or salvage immunotherapeutics for a subset of patients with the favorable *P2RX5* haplotype.

RESULTS

Human P2RX5 mRNA is selectively expressed in normal B cells and hematologic malignancies

To uncover novel, preferably multi-lineage immunotherapy targets, we surveyed publicly accessible single-cell RNA sequencing (scRNA-seq) data from the Human Protein Atlas (HPA, version 24 [42]), the Tabula Sapiens portal [43], and the MMRF Myeloma Immune Atlas [44] . As CD19 is part of Tabula Sapiens cluster 70 “Lymphoid tissue - Immune response”, we examined all genes in that cluster, prioritizing those with high levels of expression in lymphoid malignancies and minimal expression in non-lymphoid tissues.

We found that *P2RX5* mRNA was elevated in B- and plasma cells but minimal in all other cell types (**Figures 1A and S1A, B**). This B-cell-specific expression pattern was also observed in the RNA-seq data of various immune cell subsets sorted from human blood (**Figures 1B and S2A**) [42,45], as well as bone marrow (**Figure 1C, right**) and tonsils (**Figure 1C, right**) profiled in our previous studies [46,47] . Specifically, during early B-cell development in the bone marrow, *P2RX5* was absent in early progenitors and CD34+ pro-B lymphocytes but upregulated upon differentiation into pre-B-lymphocytes and immature B cells (**Figure 1C)**.

In bulk RNA-seq of human tissues, the highest *P2RX5* levels occur in B-cell-rich tissues such as the lymph nodes, tonsils, spleen, appendix and small intestines; with little to no expression across other human tissue sites (see **Figure 1D** for the Genotype-Tissue Expression (GTEx) cohort [48], as implemented by the UCSC Toil RNA-seq recompute compendium [49] and **Figure S2B** for the Human Protein Atlas cohort [42]). This mirrored the tissue expression pattern for other B-cell markers such as CD19, CD20 and CD79B. This elevated P2RX5 expression is retained by neoplastic diffuse large B-cell lymphoma (DLBCL) and ALL cells, relative to non-lymphoid normal human tissues (**Figure 1D**). Across species, human P2RX5 expression is distinct from its orthologs: murine *P2rx5* is highest in brown adipose and cardiac tissues with minimal splenic expression, while simian *P2rx5* peaks in the brain and cardiac tissues **(Figure S2C)** (GEO dataset GSE219045 [50]).

Microarray data from the HEMAP portal [51] largely agreed with our RNA-seq findings. Compared to non-cancerous stem, erythroid, myeloid and T-lymphoid cells, *P2RX5* mRNA levels were elevated in non-cancerous B-lymphoid cells as well as B-cell neoplasms (B-ALL, BCL, and chronic lymphocytic leukemias (CLL)) and multiple myeloma (**Figure 1E**). Surprisingly, there were relatively high *P2RX5* mRNA levels in T-ALL compared to their normal cells of origin (i.e., T-lymphoid; **Figure 1E**).

Gene polymorphisms result in multiple isoforms of P2RX5 mRNA

Given that multiple P2RX5 isoforms are annotated in GENCODE v49 [52], we reanalyzed Cancer Cell Line Encyclopedia (CCLE) RNA-seq data [53] to determine which isoforms of P2RX5 were expressed most abundantly. We also performed Oxford Nanopore long-read direct RNA sequencing on the Raji and Reh Burkitt’s lymphoma cell lines, to obtain end-to-end sequences of *P2RX5* transcripts that were free of potential cDNA-seq artifacts reported by us previously [54] (**Figure 2A**). In these and other BCL cell lines with high levels of *P2RX5* mRNA expression, we identified up to 5 different transcript variants arising due to gene polymorphisms and alternative splicing of exons 3 and 10 (**Figure 2B**). The longest was dubbed ‘full-length’, or *P2RX5-FL* isoform. Still, in cell lines with the *rs3215407* ‘alt’ allele (delG, or single G deletion) in exon 3 it encodes a C-terminally truncated protein isoform (ΔC). However, this frameshift mutation is “rescued” as a result of exon 3 skipping, which occurs at a low frequency (<20%) across all samples, either alone (Δ3) or with concomitant skipping of exon 10 which removes one of the two transmembrane domains (Δ3Δ10). Consequently, the predominant P2RX5 isoforms found in BCL cell lines were all exon 3-containing, namely FL, Δ10 and ΔC (**Figure 2C**).

To create an orthogonal method to detect exon 10 skipping (Δ10) or inclusion (∇10), we first designed appropriate DNA cassettes and exon-specific qPCR primers to discriminate between P2RX5-FL and Δ10 isoforms, with an additional primer pair amplifying constitutive exon 9 (**Figure S3A**). The use of these reagents allowed accurate quantification of this alternative splicing event in single- and mixed-template qPCR reactions (**Figure S3, B and C**). In RT-qPCR assays, these primers detected exon 10 inclusion in Daudi and Raji cells, as well as exon-10 skipping in Ramos and DOHH2 cells (**Figure S3D**), which was consistent with the RNA-seq data (**Figure 2C**).

Over 80% of people of African descent express the full-length isoform of P2RX5 (P2RX5-FL)

Exon 10 was constitutively included in all cell lines homozygous for the ancestral rs891746 (A) allele (e.g., Daudi, Raji, MM.1s and RPMI-8226) but completely skipped in those homozygous for the reference (C) allele (e.g., DoHH2, Ramos and Reh) (**Figure 2C and S3D**). This was likely due to the fact that the C allele (and the complementary G on the opposite strand) disrupts the canonical 5' splice site dinucleotide, GT, in the downstream intron 10 (**Figure 2A**). While the A allele had been previously linked to exon 10 inclusion in LCL samples [55], we extended this linkage to all normal tissues, including splenocytes, using Splicing Quantitative Trait Loci (sQTL) analysis implemented in GTEx [56] (**Figure 2D**). Additionally, the effect of the rs891746 SNP on exon 10 splicing was experimentally validated with minigene reporters in Raji and OCI-Ly8 cells (**Figure 2E, top**). Under all conditions, the C allele produced shorter, exon 10-skipping and the A allele - longer, exon 10-including transcripts (**Figure 2E, bottom**).

Additionally, all cell lines that expressed the P2RX5-FL variant were from donors of African (AF) ancestry. Thus, we investigated the prevalence of the rs891746 ancestral allele in various human populations. According to aggregate data from the NCBI Allele Frequency Aggregator (ALFA) project [www.ncbi.nlm.nih.gov/snp/docs/gsr/alfa/], the ancestral rs891746 A allele was exceedingly rare in European, Asian, and Latin American individuals. In contrast, up to 80% of AF donors maintain the reading frame in both copies of their *P2RX5* gene by being homozygous for the rs3215407([G]5) allele while inheriting at least one copy of the rs891746 A-allele (**Figure 2F**). Owing to linkage disequilibrium, the rs891746 A allele also had a 97% co-occurrence rate with the rs3215407 [G]5 allele (**Figure 2G**), suggesting that 97% of AF individuals contain at least one functional copy of *P2RX5*.

This P2RX5-FL variant was also detected in >75% of MM patients of AF ancestry from the MMRF CoMMpass study [57] and endemic Burkitt's lymphoma (eBL) patients from West Kenya [58] and Uganda [59,60] (**Figure 2H**). Of note, for MM patients of AF ancestry in the CoMMpass study, Kaplan-Meier analysis revealed an inverse relationship between the number of P2RX5-FL copies and survival probability, with homozygous (+/+) patients showing the shortest overall survival (**Figure 2I**). For healthy tissues, P2RX5 expression pattern in samples homozygous for P2RX5-FL was indistinguishable from that seen in the broader GTEx population, both displaying elevated transcript levels in spleen, EBV-transformed lymphocytes and small intestine (**Figure S3E**). This suggests that the P2RX5-FL variant retains B-cell lineage-restricted expression in normal tissue while serving as a risk allele in plasma cell malignancies.

P2RX5-FL-encoded protein is stable and properly N-glycosylated

Commercially available anti-P2RX5 antibodies do not recognize their cognate target in its native conformation. To generate P2RX5-reactive mAbs suitable for flow cytometry, we immunized mice with P2RX5-FL-overexpressing syngeneic NIH-3T3 cells and generated multiple hybridomas. Of them, 1D9 produce an antibody that detected, in both immunoblotting and flow cytometric assays, human and simian P2RX5 overexpressed in Ramos BCL and Jurkat T cells - but not their murine ortholog (**Figure S4A and B**). This species specificity suggested that 1D9 recognizes amino acids shared by human and simian P2RX5 but not murine P2rx5. After performing the extensive mutagenesis screen, we discovered that substituting the single lysine-131 in human P2RX5 to the glutamate found in murine P2rx5 (K131E), was sufficient to abolish the interaction between the mutant and 1D9 in overexpression studies (**Figure S4C)**. Conversely, introducing the reciprocal E131K substitution into murine P2rx5, "rescued" 1D9 binding to the mutant protein (**Figure S4D**). The likely linear nature of the 1D9 epitope makes the corresponding antibody suitable for a variety of assays, including glycosylation and protein stability studies.

We first used 1D9 to perform immunoblotting on four cancer cell lines with endogenous P2RX5-FL mRNA expression (Daudi, Raji, MM.1s, and RPMI-8226). In these cells, 1D9 detected a ~60 kDa protein (**Figure 3A, left**). The specificity of detection was established by knocking out P2RX5 using CRISPR-Cas9 technology (**Figure S4E and 3A, right**) and through the use of transient transfection with various P2RX5-overexpressing vectors (**Figure 3B**). While the predicted molecular mass of P2RX5 is 49.3 kDa, glycosidase treatment (**Figure S4F**) and N77A/N202A mutagenesis (**Figure S4G**) revealed that N-linked glycosylation at N77 and N202 accounts for the discrepancy in electrophoretic mobility.

Surprisingly, despite high Δ10 *P2RX5* mRNA levels in DoHH2 cells (**Figure 2C and S3D**), little to no P2RX5 protein was detected using immunoblotting (**Figure 3A, left**). Similarly, Raji cells overexpressing the FL variant made markedly more protein than those overexpressing Δ10 or Δ3Δ10 (**Figure 3B, right**),

despite comparable levels of pan-P2RX5 mRNA (**Figure 3B, left**). Since amino acids encoded by exon 10 constitute one of the two transmembrane, pore-forming domains of P2RX5 (**Figure 2B, right**), we reasoned that exon 10 skipping could destabilize P2RX5 protein, leading to its rapid degradation. Indeed, once new protein synthesis was inhibited by cycloheximide, flow cytometric assays detected more rapid loss of the green fluorescent protein (GFP)-tagged version of Δ10 relative to the FL isoform, (**Figure 3C**).

P2RX5FL protein is selectively expressed in normal and malignant B cells

We further used 1D9 for IHC staining of formalin-fixed paraffin-embedded (FFPE) sections, to spatially profile P2RX5 protein expression in normal human tissues and BCL samples of defined P2RX5 genotypes. Across sections of P2RX5 FL/FL and FL/Δ10 lymph nodes and spleens, P2RX5 was detectable strictly in the B-cell compartment of germinal centers, co-localizing with CD20 (**Figure 3D**). No staining was apparent in the skeletal muscle used as a negative control, fully consistent with RNA-seq data (**Figures 1 and S1**). 1D9 also robustly stained xenografts of P2RX5-FL-positive Raji cells but not their P2RX5 KO derivatives (**Figure 3E**). Importantly, uniform P2RX5 staining was apparent on two archival BCL samples with the P2RX5 FL/FL and FL/ΔC genotypes, but not on the BCL sample with the ΔC/ΔC genotype (**Figure 3F**).

P2RX5FL is robustly expressed on the surface of BCL, MM, and T-ALL cells

To establish that P2RX5-FL localizes to the cell surface in blood cancer cells, we inserted the FLAG tag into predicted extracellular loops of various P2RX5 variants (**Figure 4A**) and overexpressed the recombinant constructs in Raji and Ramos cells, confirming expression by RT-PCR (**Figure 4B, top**). Only in the case of P2RX5-FL were live, non-permeabilized cells strongly positive for surface FLAG in flow cytometry (**Figure 4B, bottom**). We also generated a knock-in (KI) construct, wherein the FLAG-tag coding sequence was inserted into the endogenous *P2RX5* gene in Raji cells using CRISPR-Cas9 engineering. After confirming insertion via RT-PCR and amplicon sequencing (**Figure 4C**, **top**), we performed flow cytometric staining and once again observed strong positivity, with parental and P2RX5 KO cells serving as negative control (**Figure 4C**, **bottom**).

The cell-surface expression of P2RX5-FL was additionally verified through direct staining with another anti-P2RX5 hybridoma clone, 2F4. In live-cell flow cytometry assays, both mAbs stained cells with P2RX5-FL expression, both endogenous (Raji and MM.1s) and ectopic (Ramos transfectants) (**Figure 4D**). Of note, these antibodies were non-competing, as preincubation of Raji and Daudi cells with unlabeled 1D9, did not inhibit subsequent staining by fluorophore-labelled 2F4, and vice versa (**Figure 4E**). We also used flow cytometric staining to calculate binding affinities of 1D9 and 2F4. These values were marginally higher for 1D9 (EC50 ≈45 nM) relative to 2F4 (EC50 ≈65 nM) across both endogenous (**Figure 4F**) and overexpression (**Figure S5A**) models. No measurable binding to Raji P2RX5 KO and parental Ramos cells was detected (**Figures 4F and S5A**). Nor did these antibodies stain HEK293T cells overexpressing other P2RX family members (**Figure 4G**), further attesting to their specificity.

Using the higher-affinity 1D9 clone, we performed antibody binding capacity (ABC) assays to quantify P2RX5 surface density. Cell lines homozygous for P2RX5-FL (including Raji, Daudi, MM.1s, RPMI-8226, and a lymphoblastoid cell line [LCL] from an AF donor) averaged 3,000–6,000 P2RX5 molecules per cell (**Figure 4H)**. This was lower than the 40,000-100,000 CD19 molecules per cell detected for the LCL, Raji and Daudi cells but comparable to ≈6,000 BCMA molecules per cell expressed by MM.1s and RPMI-8226 cells (**Figure 4H**). ≈1,000 P2RX5 molecules was detected on the heterozygous P2RX5 FL/ΔC MOLT-16 T-ALL cells, and less than 300 P2RX5 molecules – on P2RX5 Δ10/Δ10 DoHH2 and ΔC/ΔC Ramos cells (**Figure 4H)**. These P2RX5 surface densities were consistent with our earlier immunoblotting data (**Figure 3A**).

In addition to cell lines, we stained live cells from bone marrow aspirates from T-ALL and MM patients with 1D9 and 2F4. All 5 aspirates from AF donors were found by RT-qPCR and TaqMan SNP genotyping assays to express at least one copy of P2RX5-FL. Consistent with this finding, we readily detected $CD7^{+}P2RX5^{+}$ T-ALL cells and $CD138^{+}P2RX5^{+}$ double-positive MM cells in these five cases (**Figure 4I**) – but not in the case of one P2RX5 ΔC/ΔC donor (MM-3).

P2RX5 FL expression is undiminished by the loss of other immunotherapy targets or exposure to most blood cancer therapeutics

To investigate P2RX5-FL expression in lymphoid and multiple myeloma models of antigen escape, we knocked out CD19, CD20, CD22, and CD79B in Raji and Daudi BCL cells and BCMA and CD38 – in MM.1s and RPMI-8226 cells. We then confirmed epitope loss by flow cytometry and simultaneously stained KO cells for P2RX5. In none of these cell lines was P2RX5 surface expression lost (**Figure S5B**). Conversely, P2RX5 knockout didn't affect positivity for any of these markers in parental cells (**Figure S5C**), suggesting P2RX5-FL could be used either as a first-line immunotherapy target or as a target for salvage immunotherapy.

Since potential P2RX5-directed immunotherapeutics are likely to be tested in patients with prior exposure to chemotherapy, we measured the effect of common anti-cancer drugs on P2RX5 expression. Specifically, we treated Raji and Daudi cells with doxorubicin and vincristine, MM.1s and RPMI-8226 cells - with bortezomib and lenalidomide, and all 4 lines - with dexamethasone. The drug concentrations were chosen to result in measurable reduction in cell viability (bar graphs in **Figure S5D and E**). We observed that transient exposure to doxorubicin, vincristine, bortezomib, and lenalidomide had no effect on P2RX5 levels (**Figure S5D**). Of note, treatment with the corticosteroid dexamethasone led to elevated P2RX5 expression in all four cell lines tested, with close to a two-fold increase in median fluorescence intensity (MFIs) in MM.1s and Raji cells (**Figures 4J and S5E**).

A P2RX5-CD3-directed bispecific antibody enable killing of BCL and MM cells.

To evaluate the potential of P2RX5-directed immunotherapeutics, we tested several prototype bispecifics based on 1D9- or 2F4-derived scFvs in the backbone of the CD19/CD3-targeting bispecific T-cell engager (BiTE) blinatumomab [61]. Among these, a 2F4-equipped bispecific, dubbed αP2RX5-αCD3 (**Figures 5A and S6**), displayed the most potency *in vitro* (**Figure 5B)**. When added to 5-day co-cultures of Raji-CD19 KO target cells admixed with T cells from 3 individual donors, αP2RX5-αCD3 induced robust T-cell expansion and complete lysis of P2RX5-FL-positive Raji cells, regardless of P2RX5 genotypes of the effector cells (**Figure 5C**). As expected, no T-cell expansion occurred without target cells.

In similarly designed 1-day co-culture assays, we directly compared αP2RX5-αCD3 to the αCD19 BiTE and discovered that it has sub-picomolar potency (EC50: 0.24 pM), which was comparable to that of blinatumomab (EC50: 0.17 pM). As a result, it effectively lysed multiple endogenous P2RX5-FL-expressing cell lines (Raji, Ramos-P2RX5-FL, MM.1s, and RPMI-8226) while Raji-P2RX5-KO cells and ΔC/ΔC RamosPuro cells were spared (**Figure 5D**). Of note, pretreatment of MM.1s target cells with dexamethasone, which upregulates P2RX5 expression on the cell (**Figure 4J and S5E**), further enhanced the cytolytic activity elicited by αP2RX5-αCD3 (**Figure 5E**).

To test the feasibility of dual-targeting CD19 and P2RX5, we used a bicistronic lentiviral expression vector (dubbed αCD19-28z.αP2RX5-αCD3) to generate donor T cells that simultaneously express CD19-directed chimeric antigen receptor (CAR) and secrete αP2RX5-αCD3 (**Figure 5F**). These cells were co-cultured for 1-5 days with target Raji cells, either wild-type or CD19 KO (**Figure 5G**). Unlike the monospecific αCD19-28z CAR T cells, which only killed wild-type Raji cells, the αP2RX5-αCD3-armed CAR T cells killed Raji cells without regard for CD19 expression (**Figure 5H and I**).

To test its utility against CD19-negative disease *in vivo*, we intravenously injected luciferase-expressing (luc+) Raji CD19 KO cells into NSG mice and allow cell line-derived xenografts (CDXs) to establish for 7 days. Then the animals were randomized into three groups, to receive either mock-transduced donor T cells, T cells expressing the CD19 CAR, or CAR T cells additionally armed with αP2RX5-αCD3. Disease spread was assessed 17 days later using optical imaging. We observed that while monospecific CAR T cells were completely ineffective in controlling growth of CD19-negative Raji cells, αP2RX5-αCD3-armed CART-19 cells markedly delayed disease progression, even in the presumed absence of CAR T cells activation expansion by normal and neoplastic B cells (**Figure 5J**).

P2RX5-redirected CAR T cells have therapeutic efficacy in MM preclinical models.

Because CAR T cells have proven their utility in MM patients, we designed several 1D9 scFv-based second-generation CARs containing CD3ζ activation domain and either CD28 or 4-1BB costimulatory

domains (dubbed αP2RX5-28z and αP2RX5-BBz, respectively) (**Figure 6A**). These cassettes were inserted into lentiviral vectors and used to transduce donor T cells. As a result, more than 30% of donor T cells stained positive for the CAR construct in flow cytometry assays (**Figure 6B**). The choice of CAR did not noticeably affect T cells expansion over 16 days, which was comparable to that of the control αCD19-28z CAR T cells (**Figure 6C**). Furthermore, in cell avidity assays, more the 70% of both αP2RX5 CAR T cells remained bound to target RPMI-8226 cells at the end of the force curve, relative to the 30% remaining observed for the mock transduced T cells (**Figure 6D**). This suggests that the expression of either αP2RX5-BBz or -28z by T cells enhanced cell avidity towards P2RX5FL-positive target RPMI-8226 cells.

To assess their cytolytic activity, αP2RX5-28z and -BBz CAR T cells were co-cultured for 5 days with LCLs derived from the same P2RX5-FL/FL donor (**Figure 6E**). Relative to mock-transduced T-cell co-cultures, there were comparable 2-fold increases in CAR T cell counts and 60% reductions in viable LCL cell counts (**Figure 6F**). Similar modest levels of killing were observed with B-lymphoid Raji and Daudi cells; however, MM.1s and MOLT-16 cells were much more sensitive, with percentages of surviving cells in single digits, even after the knockout BCMA (**Figure 6G and H**). Pretreating MM.1s cells with dexamethasone further enhanced αP2RX5-BBz CAR-mediated cytolysis (**Figure 6I**). In the same set of experiments, we also tested CAR T cells of different P2RX5 genotypes (FL/FL, Δ10/Δ10, and ΔC/ΔC) in 1- and 4-day co-cultures and didn't observe any appreciable differences with either P2RX5 CAR construct (**Figure 6G**).

Finally, we evaluated P2RX5-directed CARs in vivo using an orthotopic mouse model of MM. In this model, luc+ RPMI-8226 cells were injected into the femur of NSG mice and CDXs were allowed to establish, as described previously [62] (**Figure 6J**). Then 0.8×10^6 CAR-positive T-cells were infused into tumor-bearing mice, and their expansion and persistence were followed by collecting peripheral blood samples at days 9, 17, 27, and 91, and quantifying human T cell levels with flow cytometry. We observed that both P2RX5 CAR T cell products persisted for at least 3 months post-infusion at levels comparable to that of the commercial BCMA CAR ciltacabtagene autoleucel (**Figure 6K**). Most importantly, compared to the mock T-cell cohort, a single i/v dose of αP2RX5-28z, αP2RX5-BBz, or αBCMA-BBz CAR T cells effectively controlled tumor growth **(Figure 6L)** and extended survival beyond 100 days **(Figures 6M),** with αP2RX5-BBz driving significantly longer survival compared to αP2RX5-28z ($p=0.04$) and being non-inferior to the current clinical gold standard αBCMA-BBz.

DISCUSSION

Most lymphoid malignancies have low mutation burden [63], which makes them largely invisible to the adaptive immune system trained to recognize non-self-antigens. Therefore, immune checkpoint inhibitors have limited utility in liquid cancers; instead, current FDA-approved immunotherapies target not cancer-specific, but rather lineage markers, such as B cell-specific CD19, CD20, and CD22, and plasma cell-specific B Cell Maturation Antigen (BCMA) [64]. The rapid emergence of bispecific T cell engagers and especially CAR T cells 10+ years ago raised hopes that even chemotherapy-resistant lymphoid cancers can be cured. Indeed, initial response rates in heavily pre-treated populations often exceeded 80% [65]. However, more recently it became apparent that antigen escape is a major cause of treatment failure, sharply limiting progression-free and overall survival [10,17]. This underscores the need for diversified target repertoires for both salvage and combination therapies. Yet the apparent paucity of true lineage-restricted surface markers limits the discovery of new targets.

It has been proposed that RNA dysregulation, in particular alternative splicing, could be a rich source of unique proteoforms [66-68]. For example, our earlier work has shown that in pediatric B-ALL there is an abundance of non-canonical transcripts [46,69], including those corresponding to classical immunotherapy targets like CD19 [14-16] and CD22 [29]. We further demonstrated that highly specific antibodies can be generated against such proteoforms, for example the CD22 Δex5-6 variant [29]. Here, by focusing on genetic determinants of alternative splicing, we were able to identify a protein that is both a novel B-cell lineage marker and a compelling multilineage immunotherapy target: P2RX5.

The previous lack of attention to this protein is due to the common perception that in humans P2RX5 exists as a natural deletion mutant lacking amino acids 328-349 of exon 10, which in other species contribute to transmembrane domain 2. This event could be detrimental to protein expression-structure-

transport to the membrane. In fact, previous reports had suggested that the Δex10 variant is predominantly intracellular [55,70]. Our data shows that at least in B cells instead of accumulating in the cytosol, the truncated protein is rapidly degraded, making the underlying event loss-of-function.

The cause of the P2RX5 Δex10 event is the prevalent polymorphism at the 5' splice site at the beginning of intron 10, replacing the canonical GT dinucleotide with GG. However, the non-reference ancestral allele (conserved in primates) is retained in >80% of patients of AF descent. Thus, although all genetic variants of P2RX5 are transcribed equally well, only the full-length transcript is likely to be of functional significance.

Furthermore, we found that in normal human tissues, P2RX5 expression is B-cell lineage-restricted. P2RX5 is upregulated early in B-cell development, beginning at the pre-B cell stage in the bone marrow, increases as B cells mature, and is downregulated after terminal differentiation into plasma cells. Our deep RNA-seq-based findings are consistent with prior RT-PCR-based reports of elevated expression of P2RX5 (a.k.a. LRH-1, a hematopoietic-lineage restricted minor histocompatibility antigen) in normal and malignant B-lymphoid tissues [71-73]. This diverges markedly from the murine ortholog of P2rx5 which is reportedly expressed in non-B-lymphoid cells such as osteoclasts, macrophages and brown adipocytes [74,75,76]. At the tissue level, elevated levels of human P2RX5 are detectable exclusively in B-cell-rich tissues such as the lymph nodes, tonsils, spleen, appendix and small intestine; while the highest levels of murine P2rx5 were detected in brown adipose and cardiac tissues with minimal expression in the spleen. The expression pattern changes again for simian P2rx5 which had the highest expression in CNS and cardiac tissues.

Not surprisingly, P2RX5 is expressed in all types of B-lymphoid malignancies of various stages of differentiation, ranging from acute lymphoblastic to chronic lymphocytic leukemia. What was surprising is the P2RX5-positivity of MM and T-ALL. Plasma cells typically lack or exhibit low expression of classical B-cell markers, such as CD19, CD20, and CD79B; and normal T cells do not stain positive for P2RX5, notwithstanding the prior report that the Δex10 variant of P2RX5 is upregulated during T-cell activation with anti-CD3/CD28 [77]. For T-ALL, this suggests that autologous P2RX5-directed CAR T cells could be efficiently generated from patients without the complications of fratricide and T-cell aplasia encountered by CAR T cells targeting typical pan-T-cell markers such as CD5 and CD7 [78,79]. Indeed, even when T cells from a P2RX5(FL/FL) donor were used, we were able to generate P2RX5-directed CAR T cells that *in vivo* expanded at rates similar to CART-19, consistent with the lack of fratricide.

In addition to CAR T cells, we also developed bispecific T cell engagers and found that both P2RX5-directed therapies were highly potent against P2RX5FL-positive BCL and MM cell lines; on par with FDA-approved CD19-directed blinatumomab and BCMA-directed ciltacabtagene autoleucel. Of note, P2RX5 expression persists after the genetic deletion of common immunotherapy targets (e.g.: CD19, CD20, CD22, CD79B, CD38 or BCMA). Conversely, the deletion of P2RX5 did not affect positivity for the same common immunotherapy targets. Thus, P2RX5 is a viable co-target in combination therapies to prevent relapses driven by single-antigen loss. Another attractive aspect of targeting P2RX5 is its upregulation during treatment with dexamethasone. This suggests that P2RX5-directed therapies could be most effective when administered alongside corticosteroids which are routinely given to patients with MM or BCL, as a direct chemotherapeutic agent or to manage inflammation, including the toxicities related to CAR T-cell therapy such as CRS or ICANS.

In summary, we have credentialled P2RX5 as a promising target for genotype-guided immunotherapy in lymphoid malignancies. While P2RX5-directed therapies would be feasible only in selected populations of AF ancestry, it is worth noting that the very same populations have benefited far less from modern forms of immunotherapy [80]. In the U.S., only 1.3% of participants in CART trials are of African ancestry even though they account for more than 25% of MM cases [81,82]. Compared to non-African populations, African Americans also have two-fold higher incidence and mortality rate for MM [83-85] and worse survival for multiple forms of lymphoid malignancies, including CLL[86,87], DLBCL[88] and follicular and marginal zone lymphoma 33864695 [88].

STUDY LIMITATIONS

Our study is primarily limited by a relatively small number of samples from donors of African ancestry. While we were able to measure P2RX5 protein levels (via flow cytometry or IHC) in several P2RX5FL-genotyped normal tissues and tumor samples, the B-cell lineage restricted expression of P2RX5 protein should be substantiated across a range of different organs from a larger cohort of P2RX5FL-genotyped donors. Although we have inferred that more than three-quarters of African patients express at least one copy of P2RX5 based on transcriptomic data, this inference needs to be validated at the protein level in more BCL, T-ALL and MM samples. Finally, our observation that an increase in P2RX5FL copy numbers was associated with worse outcomes for African patients with MM, needs to be replicated in a larger cohort of patients.

METHODS: EXPERIMENTAL MODELS

Animal models

Mice studies were carried out in accordance with Children's Hospital of Philadelphia and University of Pennsylvania Institutional Animal Care and Use Committee (IACUC) guidelines. For αP2RX5-αCD3 secreting αCD19-28z CAR T-cell experiments, 6- to 8-week-old female NSG mice were injected intravenously (IV) with $0.2x10^6$ Raji-CD19KO-luciferase-zsGreen cells on day -7. Tumor burden was determined by IVIS spectrum whole animal bioluminescent imaging on day -1. The mice were then randomized to groups with equal mean tumor burdens and a total of $0.3x10^6$ CAR T cells were IV injected into each mouse on day 0. To compare the αP2RX5-28z or -BBz CAR T cells with ciltacabtagene autoleucel, 6- to 8-week-old NSG mice were injected intraosseously with RPMI-8226-luciferase cells as described earlier [62]. After xenografts were established, mice were injected intravenously with a total of $0.8x10^6$ CAR T cells. Whole animal bioluminescent imaging was performed with a using the IVIS Lumina S5 (PerkinElmer) and the images were analyzed using Living Image, v.4.1, software (PerkinElmer). The total bioluminescent signal flux for each mouse (flank) was expressed as average radiance (photons per second per square centimeter per steradian). Survival was recorded and analyzed at the end of the study. To determine the presence of CAR T and tumor cells, peripheral blood was collected from all animals and the absolute numbers of live/human CD45+/murine CD45-/CD3+ T cells were determined by flow cytometry.

Human samples

Archival FFPE samples of donor tumor (lymphoma), lymph node, spleen and muscle tissue were obtained from the Penn Tumor Tissue/Biospecimen Bank (TTAB) under the Penn Institutional Review Board (IRB) approved protocol 856585. Cryopreserved bone marrow aspirates from Black or African American patients with T-ALL were obtained from the CHOP Center for Childhood Cancer Research Biobank and Repository under the CHOP IRB-approved protocol #10-007767. Bone marrow aspirates from Black or African American patients with MM were collected under the approved IRB protocol 842940 through the PCD group at the Hospital of the University of Pennsylvania.

Data set usage

ScRNA-seq-based normalized protein counts per million (nCPM) for P2RX5 were downloaded from the Human Protein Atlas portal (HPA, version 24) 34321199 [43]. Within each dataset, we calculated weighted mean nCPM counts for all clusters sharing a cell type, weighting by the number of cells per cluster. Clusters with mixed cell type or low-confidence cell type annotations were excluded.

The Monaco PBMC (PRJNA418779) [Ref [45]], Boultwood Bone Marrow (PRJNA473835) [Ref [89]], bone marrow and tonsil subsets (PRJNA475684) [Ref [29,46,47]], mouse and macaque tissue (GSE219045) [Ref [50]], CCLE (PRJNA523380) [Ref [53]], eBL Uganda 1 (PRJNA292327) and BL Uganda 2(PRJNA374464) [Ref [59,60]], eBL West Kenya (phs001282.V2.p1) [Ref [58]], MMRF CoMMpass (PRJNA248539) [Ref [57]] datasets were from the BioProject or dbGaP databases of the National Center for Biotechnology Information (NCBI).

METHODS DETAILS

RNA seq analyses

RNA-seq reads were first trimmed to remove adapters (BBTools v38.96) and were then aligned using STAR v2.7.9a to the hg38 reference genome while providing known gene isoforms through the GENCODE annotation V32. We used STAR flags "–quantMode GeneCounts" and "–alignSJoverhangMin 8" to quantify genes and ensure spliced reads had an overhang of at least eight bases. Junction spanning reads were obtained from the STAR "*_SJ.out.tab" result files, and each entry was normalized by dividing by the total number of junction-spanning reads and multiplying by a factor of 1 million to obtain the "junctions per million" or JPM. TPMs for all samples were calculated using TPMCalculator [90] version 0.0.3. Sample P2RX5 genotype were classified based on the ratio of [exon-10 to -11 JPM] / [exon-9 to -11 JPM] where values over 0.9 were classified as homozygous for exon-10 inclusion, in between 0.1 and 0.9 as heterozygous and below 0.1 as homozygous for exon-10 skipping. The rs3215407 alleles were determined via manual look-up of the alignments on IGV.

Plasmid constructs

The *P2RX5* minigene sequence (exons 9-11) containing truncated introns and either the rs891746(A or C) alleles was fused upstream of a NanoLuc ORF and cloned into the MXS_CMV::PuroR-bGHpA plasmid, replacing the PuroR ORF. MXS_CMV::PuroR-bGHpA was a gift from Pierre Neveu (RRID:Addgene_62439) [91]. . The pCDH-EF1 vector was a gift from Kazuhiro Oka (RRID:Addgene_72266). The pLC-Luc-IRES-zsGreen-P2A -Blast lentiviral vector was constructed by replacing the CMV promoter sequence (immediately upstream of the zsGreen ORF) in pLC-ZsGreen-P2A-Blast with the EF1a promoter, Luciferase ORF and IRES sequence of pHIV-Luc-ZsGreen. The pLC-ZsGreen-P2A-Blast plasmid was a gift from Eva Gottwein (RRID:Addgene_123322) (PMID: 29954751) while pHIV-Luc-ZsGreen was a gift from Bryan Welm (RRID:Addgene_39196).

Gene knockouts

Alt-R™ CRISPR-Cas9 sgRNAs (Integrated DNA Technologies) were complexed with Alt-R™ S.p. Cas9 Nuclease V3 (Integrated DNA Technologies). The CD38 gRNA sequence was described previously (PMID: 37171449). The resulting ribonucleoprotein complexes were transfected into the target cells using the Neon Electroporation System (Invitrogen).

DNA or RNA extraction.

Total RNAs or genomic DNA were isolated from whole cells or FFPE sample scrolls using the appropriate Maxwell® RSC simplyRNA Cells, RSC RNA FFPE, RSC Cultured Cells DNA or RSC DNA FFPE Kits (Promega).

Reverse transcription and PCR analysis

To generate cDNA, 500 ng of RNA (via NanoDrop™ 2000) were hybridized with a mixture of Oligod$(T)_{20}$ and random hexamer primers and reverse transcribed with SuperScript™ IV VILO™ Master Mix (ThermosFisher Scientific). Traditional PCR was performed using the Q5® High-Fidelity 2X Master Mix (New England Biolabs). Primers include P2RX5 CDS (1332 bp amplicon on P2RX5FL cDNA; forward: ATGGGGCAGGCGGGCTGCAAGG; reverse: TCACGTGCTCCTGTGGGGCTC) and P2RX5 FLAG-KI (forward:GGTTACCAAGACGTCGACAC; reverse:CGACATCCCAGATCCGCTG). Quantitative PCR (qPCR) was performed using PowerSYBR Green PCR Master Mix (Life Technologies) on an Applied Biosystems Viia7 machine. According to the Minimum Information for Publication of Quantitative Real-Time PCR Experiments (MIQE) guidelines [92], all primers used had efficiencies exceeding 95% and amplified single PCR products from cDNA mixtures, which was then validated via Sanger sequencing. Reference gene primers used include RPL27 (123 bp amplicon on NM_000988; forward: ATCGCCAAGAGATCAAAGATAA; reverse: TCTGAAGACATCCTTATTGACG), GAPDH (227 bp amplicon on NM_002046; forward: GAAGGTGAAGGTCGGAGTC; reverse: GGAAGATGGTGATGGGATTTC) and ACTB (121 bp amplicon on NM_001101.5; forward: GTCATTCCAAATATGAGATGCGT; reverse: GCTATCACCTCCCCTGTGTG) [93,94]. P2RX5 primers: exon-10 skipping (Δ10) (93 bp amplicon; forward: TGATGGTGAACGGCAAGGGT; reverse: CCTCGTACTTCTTGTCACGG), exon-10 inclusion (∇10) (135 bp amplicon; forward: AGTTCAGCATCATTCCCACCA; reverse: CCTCGTACTTCTTGTCACGG) and exon 9 (pan) (55 bp amplicon; forward: ATATTACCGAGACGCAGCCG; reverse:

CCCGTAGGCTTTCATCAGGG). Expression levels relative to control were calculated using the 2-ΔCT and 2-ΔΔCT methods. The data were normalized to the CT or RPL27 or when indicated, the mean CT of GAPDH, ACTB and RPL27. DNA contamination was routinely assessed via qPCR of negative control reverse transcription reactions which lacked reverse transcriptase (cycle thresholds above 35).

P2RX5 variant determination

For donor samples and cell lines, both genomic DNA and cDNA was genotyped using predesigned Taqman probes (Thermo Fisher Scientific. C___8728453_10 for rs891746.). RT-qPCR was also performed to determine if pan P2RX5 mRNA was upregulated, and if exon-10 was included or skipped. For cell lines, genomic DNA was also genotyped using PCR amplification followed by Sanger sequencing for rs3215407 (251 bp amplicon; forward: GCCCTCTTTCAGGTAACGCT; reverse: GGAGTGGACAGACACCCTTG) and rs891746 (231 bp amplicon; forward:TGGGGGCCCCGCTGTCCAAC; reverse:TCTTTCTGGGGGCACTGGGACAC).

Splicing minigene assay

The minigene plasmids were electroporated into Raji and OCI-ly8 cells using the Neon System (Invitrogen). Two days later, minigene transcription was analyzed via RT-qPCR and Sanger sequencing using the “minigene primers” ((495 bp amplicon; forward: ATATTACCGAGACGCAGCCG; reverse: GCCAGTCCCCAACGAAATCT)).

Antibody discovery

Anti-P2RX5 monoclonal antibodies were generated at the Fred Hutchinson Antibody Technology Core. Briefly, male and female 20-week-old mice were immunized with NIH/3T3 cells that stably overexpressed P2RX5-FL-FLAG. Following a 12+ week boosting protocol, splenocytes were isolated from high-titer-yielding mice and electrofused with FOX-NY myeloma cells. From the resulting hybridoma clones, two unique monoclonal antibody sequences, 1D9 and 2F4, were reactive to cell-surface P2RX5-FL in flow cytometry assays. 1D9 and 2F4 were produced in serum free media and purified using protein A and protein G columns on AKTA pure HPLC.

Western blotting.

Total cell lysates were prepared in Laemmli Sample Buffer (Bio-Rad) with 50 mM DTT, resolved on a 4–15% precast polyacrylamide gel (Mini-PROTEAN® TGX™, Bio-Rad) in Tris/glycine/SDS running buffer (Bio-Rad), and then transferred onto a PVDF membrane (Millipore Sigma, Immobilon-P, 0.45 µm) via the Mini Trans-Blot® Cell system (Bio-Rad). These membranes were then probed with antibodies against P2RX5 (1D9 clone), FLAG (L5 clone, Biolegend), ACTB (8H10D10 clone, Cell Signaling Technology), GAPDH (14C10 clone, Cell Signaling Technology); followed by horseradish peroxidase–linked secondary antibodies (Cell Signaling Technology). Western blot chemiluminescent signals were captured with a G:Box Chemi XX6 Gel Doc (Syngene).

Protein deglycosylation

Raji and MM.1s cell lysates (in RIPA buffer) were deglycosylated with the Protein Deglycosylation Mix II (P6044, New England Biolabs), under denaturing reaction conditions, according to the manufacturer’s protocol. The Protein Deglycosylation Mix II was replaced with water for the negative control reaction.
Experimental Model and Subject Details

Immunohistochemistry (IHC)

Formalin fixed, paraffin embedded (FFPE) section staining was performed on a Bond Max automated staining system (Leica Biosystems). Antigen retrieval was performed for 20 mins with the E2 (CD20 staining) or E1 (P2RX5 staining) retrieval solution (Leica Biosystems). For CD20 staining, we used the Bond Refine polymer staining kit (Leica Biosystems) with 1 hour room temperature primary antibody (clone L26, Dako) incubation. For P2RX5 staining, we used the ImmPRESS Excel Amplified Polymer Staining Kit, Anti-Mouse IgG, Peroxidase (MP-7602-15; Vector Laboratories) with 1 hour room temperature primary antibody (clone 1D9) incubation. Slides were rinsed, dehydrated through a series of ascending concentrations of ethanol and xylene, and then cover slipped. Stained slides were then digitally scanned at 20x magnification on an Aperio CS-O slide scanner (Leica Biosystems).

Representative pictures were taken on scanned IHC slides with Aperio ImageScope program v12.2.2.5015.

Cell culture

HEK293T cells were a kind gift from Dr. Peter Choi (Children's Hospital of Philadelphia, Philadelphia, PA). DoHH2, Ramos, MM.1s, RPMI-8226 and MOLT-16 cells were obtained from the ATCC (American Type Culture Collection). Raji cells were authenticated with short tandem repeat profiling. All cell lines were routinely tested to be Mycoplasma free via EZ-PCR Mycoplasma Detection Kit (Sartorius). DoHH2, Raji, Ramos, MM.1s, RPMI-8226 and MOLT-16 cells were maintained in RPMI-1640 medium supplemented with 10% FBS, 2 mmol/L L-alanyl-L-glutamine dipeptide at 37°C and 5% CO2. The HEK293T cells were maintained in DMEM medium supplemented with 10% FBS, 2 mmol/L L-alanyl-L-glutamine dipeptide at 37°C and 5% CO2. To generate luciferase-zsGreen reporter cell lines, cells were transduced the pLC-Luc-IRES-zsGreen-P2A -Blast lentiviral vector and cultured in 10 ug/mL Blasticidin for 3 weeks.

LCL generation.

B95-8 cells (ATCC # CRL 1612; 13) were seeded at 3 x 10^5 cells/ml in a 75cm^2 tissue culture flask in complete RPMI 1640. After two days, cells were resuspended in fresh complete RPMI 1640 at 1 x 10^6 cells/ml and stimulated with 20ng/ml tetradecanoyl phorbol acetate (TPA; Sigma-Aldrich) for 1 hour to induce virus production and then resuspended in complete RPMI 1640 for 96 hours before centrifugation at 600 g for 10 min at 4˚C. Cell supernatant was then filtered through a 0.45-micron filter and stored at -80°C. For infection with EBV, 500µl of filtered supernatant containing EBV (B95.8) was added to 5X10^6 PBMCs in 5 ml complete RPMI medium in a 25 cm^2 tissue culture flask and placed upright in a CO_2 incubator at 37°C for 2-4 hours. Subsequently, 10 ml additional medium and cyclosporin A (1µg/ml; Sigma-Aldrich, Inc., St. Louis, MO) was added. On days three and six, nine, and twelve, half of the medium was replaced with fresh complete RPMI with cyclosporin A. After two weeks, stable EBV+LCLs are formed and anti-CD19 staining was used to confirm that the culture is 100% B cells by flow cytometry.

Live-cell flow cytometry

Live cells were incubated in blocking buffer (PBS with 2% FBS, 1 mM EDTA and Human TruStain FcX™ (Biolegend)) for 20 min prior to staining with primary antibodies (i.e.: anti-FLAG, L5 clone; anti-CD19, HiB19 clone; anti-BCMA, 19F2 clone; anti-CD7, clone 4H9 and anti-CD138, clone DL-101; all from Biolegend) for 30 min. When unlabeled 1D9 or 2F4 primary antibodies were used, the blocking buffer was supplemented with 10% (v/v) goat serum (Fisher Scientific, 16-210-064) and an additional 30 min secondary antibody staining with Goat anti-Mouse IgG (H+L) Cross-Adsorbed Secondary Antibody, Alexa Fluor™ 647 (Invitrogen, A-21235), was performed. For competition assays, the blocking buffer was supplemented with 80 ug/mL of unlabeled 1D9 or 2F4 antibodies. All incubations were at 4ºC. Propidium Iodide (PI) was used to exclude dead cells from analysis. Acquisition was done on a BD Accuri™ C6 Cytometer (BD Biosciences). Manual gating was performed on the FlowJo Software v.10 (BD Biosciences). Median fluorescence intensity (MFI).

Cycloheximide chase assay

Cell lines were transduced with lentiviral particles ORFs for the indicated constructs or an empty vector control followed by 2-week selection with 10 µg/mL Puromycin (Invitrogen).
Cultured Raji cells were treated with 60 µg/mL of cyclohexmide (CHX) (Sigma-Aldrich, C1988-1G)

Manufacturing of CAR T-cells

Healthy primary human T cells were obtained from the Human Immunology Core at the University of Pennsylvania. T-cells were isolated from frozen donor PBMCs using the EasySep™ Human T-Cell Enrichment Kit (STEMCELL Technologies). Isolated T-cells were cultured in ImmunoCult™-XF T Cell Expansion Medium (STEMCELL Technologies) supplemented with 100 IU/ml of recombinant human IL-2 (Preprotech), and activated with ImmunoCult™ Human CD3/CD28 T Cell Activator (STEMCELL Technologies). Lentiviral transduction was performed the next day. The number viable cells in culture was assessed every 2 to 3 days using a Countess 3 Automated Cell Counter with tryphan blue staining and the number of population doublings was calculated. At day-7 post CD3/CD28 activation, T-cells were cryopreserved. The % of CAR positive T-cells was monitored via flow cytometry analysis upon staining with the MonoRab™ Rabbit Anti-scFv Cocktail [iFluor 647] (Genscript).

For the αP2RX5-28z/-BBz CAR T cells and ciltacabtagene autoleucel used in the intraosseous RPMI-8226 mouse xenografts models, the CAR T cells were generated as previously described [62]. Briefly, CD4+ and CD8+ cells were combined at a 1:1 ratio and activated using anti-human CD3/CD28 Dynabeads (Invitrogen, #40203D) at a 3:1 ratio. 24 hours (day 1) post activation, T cells were infected with lentiviral vectors containing the CAR transgenes (multiplicity of infection ~1.5 viral particles / T cell). Magnetic beads were removed from T cells on day 5.

Manufacturing and quantification of BiTEs

HEK293T cells that stably secrete the αP2RX5-αCD3 BiTE were generated via lentiviral transduction followed by selection with 10 µg/mL Puromycin (Invitrogen). These HEK293T-αP2RX5-αCD3 cells were expanded to confluence and left in culture for 5 days before the BiTE-containing media was concentrate with Amicon Ultra Centrifugal Filter, 50 kDa MWCO (Sigma Millipore, UFC9050). The size and concentration of the αP2RX5-αCD3 BiTE was assessed via western blotting with an anti-His-Tag antibody (Cell Signaling Technology, D3I1O clone) and a standard curve generated from Blinatumomab (MedChem Express, HY-P9963).

In vitro co-culture assays

Target luciferase reporter cells were co-cultured with expanded healthy donor T cells at 9-days post CD3/CD28 activation in the indicated effector CAR T cell or T cell to target cell (E:T) ratios for 1 or 4 days before luciferase activity was monitored with the ONE-Glo™ EX Luciferase Assay System (Promega) and a FLUOstar Microplate Reader (BMG Labtech), as a proxy for cell viability. Target cell viability and specific cytotoxicity values (%) were normalized to mock transduced T cells or T cells without bispecifc (NT) controls. In the 5-day co-culture assays, expanded T cells at day-12 post CD3/CD28 activation were co-culture with target cancer cells. Viable cell counts were determined via live-cell flow cytometry, and normalized with CountBright™ Absolute Counting Beads (Thermo Fisher Scientific). Propidium Iodide (PI) was used to exclude dead cells from analysis. APC-CD7 (Biolegend, clone 4H9), iFluor647-scFv (Genscript) and FITC-CD22 (Biolegend, clone HIB22) staining was performed to distinguish T cells (CD7+CD22-) or effector CAR T cells (scFv+CD22-) from Raji or LCL cells (CD7-CD22+).

Cell-to-cell avidity assays

Avidity was measured using the Lumicks Z-Movi assay. Z-Movi-compatible acoustofluidic chips were coated with poly-L-lysine for 3 h prior to attaching a monolayer of RPMI-8226 cells. CellTrace far-red labeled CAR T cells were allowed to incubate on the monolayer of RPMI-8226 for 10 min, and then a ramping acoustic force was applied. Cell-detachment was analyzed using ImageJ and R. Avidity experiments were conducted according to the manufacturer's (LUMICKS™) instructions.

ACKNOWLEDGMENTS

We thank past members of the Thomas-Tikhonenko laboratory, in particular Dr. Sisi Zheng and Elisabeth Gillespi for laying the foundation for this project. At CHOP, we gratefully acknowledge Paris Grimaldi and his colleagues at the Pathology Core; Florin Tuluc and his colleagues at the Flow Cytometry Core, Nicole Maertzig and her colleagues at the Department of Veterinary Resources; Kathrin M. Bernt, Matthew Tsang, and their colleagues at the Center for Childhood Cancer Research Biorepository and Registry Team. At Penn, we acknowledge the Human Immunology Core, the University Laboratory Animal Resources, and the Tumor Tissue/Biospecimen Bank (TTAB). At Fred Hutch Cancer Center, we acknowledge the staff of the Antibody Technology Core.

This work was supported by grants from the National Institutes of Health (U01 CA232563 to ATT, U01 CA232563-S3 to ATT and JBS, T32 GM135131 to JF), The V Foundation for Cancer Research (T2018-014 to ATT), and The Emerson Collective (886246066 to ATT). JBS further acknowledges support from National Science Foundation (CAREER Award 2143160), Willowcroft Foundation, and Helmsley Charitable Trust. ATT is Mildred L. Roeckle Endowed Chair in Pathology at Children's Hospital of Philadelphia and Investigator on the St. Baldrick's Foundation EPICC Team.

RESOURCE AVAILABILITY

Lead contact

Further information and requests for reagents may be directed to and will be fulfilled by the lead contact Andrei Thomas-Tikhonenko (andreit@pennmedicine.upenn.edu).

Materials availability

- The murine hybridomas will be available upon request following publication of the patent application.

Data and code availability

- Controlled access GTEx data were retrieved through dbGaP Study phs000424.v10.p2. The Genotype-Tissue Expression (GTEx) Project was supported by the Common Fund of the Office of the Director of the National Institutes of Health.
- This paper does not report any original code.
- Microphotographs and any additional information required to reanalyze the data reported in this paper are available upon request from the lead contact.

AUTHOR CONTRIBUTIONS

Conceptualization: Z.A. and A.T.T. Data curation and formal analysis: Z.A., A.C., L.P., C.S., K.E.H., F.S., M.T., D.M., P.P. and V.P. Funding acquisition: A.T.T. Investigation and methodology: Z.A., A.C., L.P., C.S., F.S., S.S., M.T., C.K., P.K.S., K.J., P.S., D.M. and P.P. Resources: Z.S.H., S.S., P.J.K, J.F., J.B.S, J.L.R, D.T.V., P.M.L. and D.A. Supervision: M.R. and A.T.T. Writing – original draft: Z.A. and A.T.T. Writing – review & editing: Z.A. and A.T.T.

DECLARATION OF INTERESTS

Z.A. and ATT are listed as co-Inventors on the patent application PCT/US2025/046721 “Antibodies and Chimeric Antigen Receptors binding to P2RX5 and Methods of Use for Treating Cancers.”

DECLARATION OF GENERATIVE AI AND AI-ASSISTED TECHNOLOGIES

During the preparation of this work, no generative AI or AI-assisted technologies have been used.

SUPPLEMENTAL INFORMATION - Supplemental Figures S1-S6

FIGURE TITLES AND LEGENDS

Figure 1. P2RX5 mRNA is selectively expressed in mature B cells and hematologic malignancies.

(A) Heatmap of P2RX5 transcript levels, expressed as normalized transcripts per million or nTPM, in various cell types (*y-axis*) identified from scRNA-seq of multiple human tissues (*x*-axis). Larger circle sizes and darker colors indicate higher P2RX5 nTPM values. Data from the Human Protein Atlas (HPA, version 24).

(B and C) P2RX5 transcript levels (TPM) in various human immune cell subsets. Cells were isolated from the peripheral blood mononuclear cell (PBMC) fraction and bone marrow via fluorescence-activated cell sorting (FACS) prior to RNA-seq.

(D) Plotted RSEM expected counts for P2RX5 in TCGA DLBCL and TARGET ALL patient samples as well as GTEx normal tissues. Shown is pre-compiled bulk RNA-seq data from the UCSC Xena portal.

(E) P2RX5 expression levels in the collated microarray data of ~10,000 normal and neoplastic leukocyte samples across all lineages, as published on the HEMAP portal.

Figure 2. four-fifths of the AF population express the full-length isoform of P2RX5 (P2RX5 FL) due to a favorable haplotype.

(A) TOP: MANE annotations of the human *P2RX5* gene exon-intron structure. MIDDLE: Sashimi plots showing read densities across all *P2RX5* exons in Raji and Reh cells. Arcs that connect exons represent splice junctions. BOTTOM: Nucleotide changes corresponding to *rs891746* SNP.

(B) LEFT: P2RX5 isoforms that arise due to the *rs3215407* indel, the *rs891746* SNP, and alternative splicing of exon 3. RIGHT: Ribbon diagram of P2RX5 full-length (FL) structure, as predicted by AlphaFold 2. Amino acids encoded by exons 3 and 10 are highlighted in green and blue, respectively.

(C) *P2RX5* isoform expression in a selection of cell lines, based on RNA-seq data. The genotype (i.e.: *rs3215407* and *rs891746* alleles), predominant isoform detected, expression levels (TPM) and exon-exon junction count per million (JPM) are shown. Exon9-exon11 junction reads are indicative of exon10 skipping while exon10-exon11 junction reads are indicative of exon10 inclusion.

(D) Normalized P2RX5 exon10 inclusion ratios in spleen (y-axis), plotted against the corresponding *rs891746* alleles (x-axis). Adapted from the GTEX portal.

(E) Splicing minigene assay. TOP: Design of minigene expression vectors containing the sequence of *P2RX5* from exons 9 to 11, with truncated introns and either the rs891746(A or C) alleles. PCR primer bindings sites are shown in green. BOTTOM: RT-PCR analysis of Raji and OCI-ly8 cell mRNA, after transfection with the minigene expression vectors or a GFP control. Control PCRs used the minigene expression plasmids as templates. Amplicons were separated by agarose gel electrophoresis and stained with EtBr.

(F) Aggregate allele frequencies for *rs3215407* across populations, as reflected in the NCBI SNP database (ALFA Project Release 4).

(G) Table displaying haplotype counts and allele frequencies for *rs3215407* and *rs891746* across all 1000 Genomes Project populations, as accessed via LDlink 5.8.0 release. Statistics are shown to the right.

(H) P2RX5 transcript levels (TPM) in MM patients of AF ancestry (MMRF CoMMpass cohort) and endemic Burkitts lymphoma (eBL) patients from Africa, based on RNA-seq analysis. Samples were stratified according the P2RX5 isoform expressed.

(I) Overall survival of MM patients with AF ancestry, stratified based on their P2RX5 isoform. Data from MMRF CoMMpass study.

Figure 3. The P2RX5FL protein has a longer half-life and is detectable in normal and malignant B cells by the monoclonal antibody, 1D9.

(A) Immunoblots of various cell line lysates, using the anti-P2RX5 mAb, 1D9. The predominant P2RX5 transcript isoform in each cell line is noted in the blue brackets.

(B) P2RX5 expression in Raji cells upon transduction with lentiviral expression vectors for the indicated P2RX5 isoforms or an empty vector negative control. LEFT: P2RX5 mRNA levels via RT-qPCR. Normalized to negative control cells. Primer binding sites are shown to the right of the graphs. RIGHT: Immunoblots of P2RX5 protein levels using the 1D9 mAb. The FL-overexpression lane contains 90% less

total cellular protein relative to other lanes to avoid signal saturation. Shown in blue is the calculated molecular weights (MW) of each overexpressed isoform based on amino acid sequence alone.

(C) Flow cytometric analysis of GFP or P2RX5(Δ10 or FL)-GFP fusion protein levels in Raji cells at various time points following cycloheximide treatment.

(D, E and F) IHC staining for CD20 and P2RX5 (using 1D9 mAb), as indicated by brown DAB chromogen staining, on FFPE sections of normal lymph nodes, spleen and skeletal muscles **(D),** Raji-WT and P2RX5 KO mouse xenografts **(E)**, as well as BCL tumor samples **(F).** Hematoxylin nuclear counterstaining in blue. *Sample *P2RX5(FL, Δ10 or ΔC)* isoform genotype, as determined by RT-qPCR and Taqman SNP genotyping assays.

Figure 4. B-cell lymphoma, MM and T-ALL samples stain positive for cell surface P2RX5FL, using the 1D9 and 2F7 monoclonal antibodies.

(A) AlphaFold prediction-based ribbon diagram of the P2RX5FL structure, with FLAG-tag insertion site highlighted in red.

(B) TOP: RT-qPCR analysis of pan-P2RX5 mRNA levels, using primers for a constitutive exon (i.e.: exon 9). Each bar represents a replicate cell sample. BOTTOM: Cell-surface FLAG expression via live-cell flow cytometry. Data from two replicate experiments.

(C) Knock-in of an extracellular FLAG-tag into the *P2RX5* gene (FLAG-KI). TOP: RT-PCR analysis of mRNA from unmodified Raji cells with wild-type *P2RX5* (P2RX5WT) or Raji FLAG-KI cells. PCR amplicons were separated by agarose gel electrophoresis and stained with EtBr. The PCR primer binding sites (which flank the FLAG insertion site) and the expected amplicon sizes are shown to the top-right. BOTTOM: Live-cell flow cytometry analysis of cell-surface FLAG expression in Raji P2RX5WT and FLAG-KI cells, as well as Raji FLAG-KI cells that had undergone *P2RX5* gene knockout (FLAG-KI + P2RX5KO).

(D, E, F, G, H, I and J) Detection of cell-surface P2RX5 via live-cell flow cytometry. The indicated cell lines were stained with unlabeled 1D9 or 2F4 mAbs followed by indirect staining with an Alexa647-labeled secondary antibody **(D)**. In competition assays, Raji and Daudi cells were pre-incubated with unlabeled 1D9, 2F4 or no blocking antibody; followed by staining with Alexa627-labeled 1D9 or 2F4 **(E).** For the antibody titration curves, parental and P2RX5KO Raji cells were stained with unlabeled 1D9 or 2F4 mAbs at the indicated concentrations prior to indirect staining with fixed concentrations of Alexa647-labelled secondary antibody **(F)**. The EC50 values were calculated from the median fluorescence intensities (MFI) of two replicate experiments **(F)**. To test antibody cross-reactivity, HEK23T cells were transfected to express FLAG-tagged P2RX1-to-7 before staining with fluorophore-labelled anti-FLAG, 1D9 and 2F4 mAbs **(G)**. The cell-surface antigen densities on cell lines, as quantified using an Antibody Binding Capacity (ABC) assay paired with fluorophore-labelled 1D9 (anti-P2RX5), anti-CD19 or anti-BCMA mAbs **(H)**. Each peak/spot represents a replicate experiment with the average density shown **(H)**. Bone marrow aspirates from patients with T-ALL **(I)** or MM **(J)**, after staining for P2RX5 with Alexa647-labeled 1D9 or 2F4. Neoplastic cell fractions were identified by positive staining for CD7 **(I)** or CD138 **(J)**, respectively. MM.1s and Raji cell lines after 3-day treatment with the indicated concentrations of Dexamethasone **(K)**.

Figure 5. The 2F4-scFv-equipped bispecific, αP2RX5-αCD3, directs T cells to lyse P2RX5-positive neoplasms.

(A) The design of αP2RX5-αCD3.

(B) Outline of ex vivo assays, performed in panels C, D and E, to evaluate αP2RX5-αCD3 activity.

(C) Flow cytometric analysis of viable T- and Raji cell counts, 5-days after the addition of the αP2RX5-αCD3 BiTE to cultures of T cells alone or in co-culture with Raji-CD19KO cells at a 2:1 ratio. Data from P2RX5 (ΔC/ΔC, Δ10/Δ10 and FL/FL) genotyped T cells are shown, each represented by a different datapoint shape and color. Cell counts normalized to no BiTE treatment (NT) controls.

(D) Target cell viability after 1-day treatment with αP2RX5-αCD3 or blinatumomab BiTEs at 0.01 pM concentration (Bar graphs on the left) or across a range of concentrations (Dose response curves on the right). Cell viabilities are normalized to the NT controls. Data from 2 different T-cell donors are shown and used to calculate the average EC50 value.

(E) Target MM.1s cell viability, after 1-day in co-culture with T cells and the indicated concentration of αP2RX5-αCD3. The MM.1s cells were pretreated for 3-days with the indicated concentration of

dexamethasone (DEX) prior to DEX washout and co-culture. Cell viabilities are normalized to the NT controls.

(F) Design of αCD19-28z.αP2RX5-αCD3 construct. Transduction with this construct leads to the generation of CD19-directed CAR T cells that secrete the αP2RX5-αCD3 BiTE.

(G) Outline of ex vivo assays, performed in panels H and I, to evaluate αCD19-28z.αP2RX5-αCD3 CAR T-cell activity.

(H and I) Mock, αCD19-28z CAR or αCD19-28z.αP2RX5-αCD3 CAR T cells were co-cultured with the indicated cell lines at the effector CAR T cell to target Raji cell (E:T) ratio of 1:1. Viable T- and Raji cell counts were assessed via flow cytometry after 5-days of co-culture **(H)**. Target Raji cell viability assessed using luciferase reporter after 1-day in co-culture **(I)**. Cell counts and viabilities were normalized to the mock transduced T-cell control. Each bar represents data from a different T-cell donor.

(J) Bioluminescent imaging of NSG mice after IV infusion with luc+ Raji CD19KO cells followed by $3x10^5$ mock transduced, αP2RX5-αCD3 or αCD19-28z.αP2RX5-αCD3 CAR T cells.

Figure 6. 1D9-scFv CAR-armed T cells display potent cytolytic activity towards P2RX5-positive neoplastic cells.

(A) Design of 1D9 scFv-based CARs (i.e.: αP2RX5-28z and -BBz).

(B) Transduction efficiency of the 1D9-scFv-based CARs into T cells, at 9-days post-transduction, via flow cytometric analysis of cell-surface scFv positivity.

(C) Population doublings of P2RX5(FL/FL)-genotype T cells after transduction with lentivirus expression vectors for either the αP2RX5-28z, αP2RX5-BBz or αCD19-28z CARs. T cells were activated with soluble anti-CD3 and -CD28, one day before transduction.

(D) Cell avidity assays. T-cell detachment from adhered RPMI-8226 targets cells, plotted against force in pN.

(E) Outline of ex vivo assays, performed in panels C, D and E, to evaluate αP2RX5-28z or -BBz CAR T-cell activity.

(F) Flow cytometric analysis of viable cell counts, after 5-day co-culture of effector T cells (mock transduced, αP2RX5-28z or αP2RX5-BBz CAR T cells) and LCLs generated from the same P2RX5(FL/FL)-genotyped donor.

(G, H and I) Viability of the indicated luc+ target cells, after 4- **(G)** or 1-day **(H and I)** in co-culture with αP2RX5-28z, αP2RX5-BBz or αCD19-28z CAR T cells. T cells from P2RX5(FL/FL), (Δ10/Δ10) and (ΔC/ΔC) donors were tested **(G)**. In panel **(I)**, MM.1s cells were pretreated for 3-days with the indicated concentration of dexamethasone (DEX), before DEX wash-out and co-culture with αP2RX5-BBz CAR T cells.

(J-M) Testing 1D9-scFv-equipped CAR T cells in a mouse xenograft model of MM. As outlined in panel **(J)**, NSG mice were implanted intratibially with luc+ RPMI-8226 cells, several days prior to IV infusion with mock, αP2RX5-28z, αP2RX5-BBz or αP2RX5-BBz CAR T cells (0.6×10^6/mouse). Disease course was assessed by following T cell persistence in the peripheral blood **(K),** tumor progression as measured by bioluminescent imaging **(L),** and overall survival **(M)**.

REFERENCES

1. Coiffier, B. (2007). Rituximab therapy in malignant lymphoma. Oncogene *26*, 3603-3613. https://doi.org/10.1038/sj.onc.1210376.
2. Marks, V.A., Latham, S.R., and Kishore, S.P. (2017). On Essentiality and the World Health Organization's Model List of Essential Medicines. Ann Glob Health *83*, 637-640. https://doi.org/10.1016/j.aogh.2017.05.005.
3. Hutchings, M., Mous, R., Clausen, M.R., Johnson, P., Linton, K.M., Chamuleau, M.E.D., . . . Lugtenburg, P.J. (2021). Dose escalation of subcutaneous epcoritamab in patients with relapsed or refractory B-cell non-Hodgkin lymphoma: an open-label, phase 1/2 study. Lancet *398*, 1157-1169. https://doi.org/10.1016/S0140-6736(21)00889-8.
4. Abramson, J.S., Ku, M., Hertzberg, M., Huang, H.Q., Fox, C.P., Zhang, H., . . . Gregory, G.P. (2024). Glofitamab plus gemcitabine and oxaliplatin (GemOx) versus rituximab-GemOx for relapsed or refractory diffuse large B-cell lymphoma (STARGLO): a global phase 3, randomised, open-label trial. Lancet *404*, 1940-1954. https://doi.org/10.1016/S0140-6736(24)01774-4.
5. Topp, M.S., Kufer, P., Gokbuget, N., Goebeler, M., Klinger, M., Neumann, S., . . . Bargou, R.C. (2011). Targeted therapy with the T-cell-engaging antibody blinatumomab of chemotherapy-refractory minimal residual disease in B-lineage acute lymphoblastic leukemia patients results in high response rate and prolonged leukemia-free survival. J Clin Oncol *29*, 2493-2498. https://doi.org/10.1200/JCO.2010.32.7270.
6. Litzow, M.R., Sun, Z., Mattison, R.J., Paietta, E.M., Roberts, K.G., Zhang, Y., . . . Tallman, M.S. (2024). Blinatumomab for MRD-Negative Acute Lymphoblastic Leukemia in Adults. N Engl J Med *391*, 320-333. https://doi.org/10.1056/NEJMoa2312948.
7. Maude, S.L., Laetsch, T.W., Buechner, J., Rives, S., Boyer, M., Bittencourt, H., . . . Grupp, S.A. (2018). Tisagenlecleucel in Children and Young Adults with B-Cell Lymphoblastic Leukemia. N Engl J Med *378*, 439-448. https://doi.org/10.1056/NEJMoa1709866.
8. Neelapu, S.S., Locke, F.L., Bartlett, N.L., Lekakis, L.J., Miklos, D.B., Jacobson, C.A., . . . Go, W.Y. (2017). Axicabtagene Ciloleucel CAR T-Cell Therapy in Refractory Large B-Cell Lymphoma. N Engl J Med *377*, 2531-2544. https://doi.org/10.1056/NEJMoa1707447.
9. Abramson, J.S., Palomba, M.L., Gordon, L.I., Lunning, M.A., Wang, M., Arnason, J., . . . Siddiqi, T. (2020). Lisocabtagene maraleucel for patients with relapsed or refractory large B-cell lymphomas (TRANSCEND NHL 001): a multicentre seamless design study. Lancet *396*, 839-852. https://doi.org/10.1016/S0140-6736(20)31366-0.
10. Majzner, R.G., and Mackall, C.L. (2018). Tumor Antigen Escape from CAR T-cell Therapy. Cancer Discov *8*, 1219-1226. https://doi.org/10.1158/2159-8290.CD-18-0442.
11. Chong, E.A., Ruella, M., Schuster, S.J., and Lymphoma Program Investigators at the University of, P. (2021). Five-Year Outcomes for Refractory B-Cell Lymphomas with CAR T-Cell Therapy. N Engl J Med *384*, 673-674. https://doi.org/10.1056/NEJMc2030164.
12. Orlando, E.J., Han, X., Tribouley, C., Wood, P.A., Leary, R.J., Riester, M., . . . Winckler, W. (2018). Genetic mechanisms of target antigen loss in CAR19 therapy of acute lymphoblastic leukemia. Nat Med *24*, 1504-1506. https://doi.org/10.1038/s41591-018-0146-z.
13. Bagashev, A., Sotillo, E., Tang, C.H., Black, K.L., Perazzelli, J., Seeholzer, S.H., . . . Thomas-Tikhonenko, A. (2018). CD19 Alterations Emerging after CD19-Directed Immunotherapy Cause Retention of the Misfolded Protein in the Endoplasmic Reticulum. Mol Cell Biol *38*, e00383-00318. https://doi.org/10.1128/MCB.00383-18.
14. Sotillo, E., Barrett, D.M., Black, K.L., Bagashev, A., Oldridge, D., Wu, G., . . . Thomas-Tikhonenko, A. (2015). Convergence of Acquired Mutations and Alternative Splicing of CD19 Enables Resistance to CART-19 Immunotherapy. Cancer Discov *5*, 1282-1295. https://doi.org/10.1158/2159-8290.CD-15-1020.
15. Asnani, M., Hayer, K.E., Naqvi, A.S., Zheng, S., Yang, S.Y., Oldridge, D., . . . Thomas-Tikhonenko, A. (2020). Retention of CD19 intron 2 contributes to CART-19 resistance in leukemias with subclonal frameshift mutations in CD19. Leukemia *34*, 1202-1207. https://doi.org/10.1038/s41375-019-0580-z.
16. Cortes-Lopez, M., Schulz, L., Enculescu, M., Paret, C., Spiekermann, B., Quesnel-Vallieres, M., . . . Konig, J. (2022). High-throughput mutagenesis identifies mutations and RNA-binding proteins controlling CD19 splicing and CART-19 therapy resistance. Nat Commun *13*, 5570. https://doi.org/10.1038/s41467-022-31818-y.
17. Zheng, S., Asnani, M., and Thomas-Tikhonenko, A. (2019). Escape From ALL-CARTaz: Leukemia Immunoediting in the Age of Chimeric Antigen Receptors. Cancer J *25*, 217-222. https://doi.org/10.1097/PPO.0000000000000381.
18. Lamble, A.J., Moskop, A., Pulsipher, M.A., Maude, S.L., Summers, C., Annesley, C., . . . Shah, N. (2023). INSPIRED Symposium Part 2: Prevention and Management of Relapse Following Chimeric Antigen Receptor T Cell Therapy for B Cell Acute Lymphoblastic Leukemia. Transplant Cell Ther *29*, 674-684. https://doi.org/10.1016/j.jtct.2023.08.030.

19. Brivio, E., Locatelli, F., Lopez-Yurda, M., Malone, A., Diaz-de-Heredia, C., Bielorai, B., . . . Zwaan, C.M. (2021). A phase 1 study of inotuzumab ozogamicin in pediatric relapsed/refractory acute lymphoblastic leukemia (ITCC-059 study). Blood *137*, 1582-1590. https://doi.org/10.1182/blood.2020007848.
20. Kantarjian, H.M., DeAngelo, D.J., Stelljes, M., Martinelli, G., Liedtke, M., Stock, W., . . . Advani, A.S. (2016). Inotuzumab Ozogamicin versus Standard Therapy for Acute Lymphoblastic Leukemia. N Engl J Med *375*, 740-753. https://doi.org/10.1056/NEJMoa1509277.
21. Loh, M.L., Gore, L., Raetz, E.A., Devidas, M., Militano, O., Borowitz, M.J., . . . O'Brien, M.M. (2019). A Phase 2 Trial of Inotuzumab Ozogamicin (InO) in Children and Young Adults with Relapsed or Refractory (R/R) CD22+ B-Acute Lymphoblastic Leukemia (B-ALL): Results from Children's Oncology Group Protocol AALL1621. Blood *134*, 741-741. https://doi.org/10.1182/blood-2019-128977.
22. Summers, C., Baxter, B., Annesley, C., Yokoyama, J., Rhea, S., Huang, W., . . . Gardner, R.A. (2021). CD22 CAR Optimization for Improved in-Human Activity Following Inadequate CD22 CAR Activity in Phase 1 Clinical Trial PLAT-04. Blood *138*, 403-403. https://doi.org/10.1182/blood-2021-147928.
23. Frank, M.J., Baird, J.H., Kramer, A.M., Srinagesh, H.K., Patel, S., Brown, A.K., . . . Miklos, D.B. (2024). CD22-directed CAR T-cell therapy for large B-cell lymphomas progressing after CD19-directed CAR T-cell therapy: a dose-finding phase 1 study. Lancet *404*, 353-363. https://doi.org/10.1016/S0140-6736(24)00746-3.
24. Fry, T.J., Shah, N.N., Orentas, R.J., Stetler-Stevenson, M., Yuan, C.M., Ramakrishna, S., . . . Mackall, C.L. (2018). CD22-targeted CAR T cells induce remission in B-ALL that is naive or resistant to CD19-targeted CAR immunotherapy. Nat Med *24*, 20-28. https://doi.org/10.1038/nm.4441.
25. O'Brien, M.M., Ji, L., Shah, N.N., Rheingold, S.R., Bhojwani, D., Yuan, C.M., . . . Loh, M.L. (2022). Phase II Trial of Inotuzumab Ozogamicin in Children and Adolescents With Relapsed or Refractory B-Cell Acute Lymphoblastic Leukemia: Children's Oncology Group Protocol AALL1621. J Clin Oncol *40*, 956-967. https://doi.org/10.1200/JCO.21.01693.
26. Zhao, Y., Short, N.J., Kantarjian, H.M., Chang, T.C., Ghate, P.S., Qu, C., . . . Mullighan, C.G. (2024). Genomic determinants of response and resistance to inotuzumab ozogamicin in B-cell ALL. Blood *144*, 61-73. https://doi.org/10.1182/blood.2024023930.
27. Shah, N.N., Highfill, S.L., Shalabi, H., Yates, B., Jin, J., Wolters, P.L., . . . Fry, T.J. (2020). CD4/CD8 T-Cell Selection Affects Chimeric Antigen Receptor (CAR) T-Cell Potency and Toxicity: Updated Results From a Phase I Anti-CD22 CAR T-Cell Trial. J Clin Oncol *38*, 1938-1950. https://doi.org/10.1200/JCO.19.03279.
28. Schultz, L.M., Jeyakumar, N., Kramer, A.M., Sahaf, B., Srinagesh, H., Shiraz, P., . . . Muffly, L. (2024). CD22 CAR T cells demonstrate high response rates and safety in pediatric and adult B-ALL: Phase 1b results. Leukemia *38*, 963-968. https://doi.org/10.1038/s41375-024-02220-y.
29. Zheng, S., Gillespie, E., Naqvi, A.S., Hayer, K.E., Ang, Z., Torres-Diz, M., . . . Thomas-Tikhonenko, A. (2022). Modulation of CD22 Protein Expression in Childhood Leukemia by Pervasive Splicing Aberrations: Implications for CD22-Directed Immunotherapies. Blood Cancer Discov *3*, 103-115. https://doi.org/10.1158/2643-3230.BCD-21-0087.
30. Bayles, I., and Milcarek, C. (2014). Plasma cell formation, secretion, and persistence: the short and the long of it. Crit Rev Immunol *34*, 481-499. https://doi.org/10.1615/critrevimmunol.2014012168.
31. Smith, E.L., Harrington, K., Staehr, M., Masakayan, R., Jones, J., Long, T.J., . . . Brentjens, R.J. (2019). GPRC5D is a target for the immunotherapy of multiple myeloma with rationally designed CAR T cells. Sci Transl Med *11*. https://doi.org/10.1126/scitranslmed.aau7746.
32. Berdeja, J.G., Madduri, D., Usmani, S.Z., Jakubowiak, A., Agha, M., Cohen, A.D., . . . Jagannath, S. (2021). Ciltacabtagene autoleucel, a B-cell maturation antigen-directed chimeric antigen receptor T-cell therapy in patients with relapsed or refractory multiple myeloma (CARTITUDE-1): a phase 1b/2 open-label study. Lancet *398*, 314-324. https://doi.org/10.1016/S0140-6736(21)00933-8.
33. Munshi, N.C., Anderson, L.D., Jr., Shah, N., Madduri, D., Berdeja, J., Lonial, S., . . . San-Miguel, J. (2021). Idecabtagene Vicleucel in Relapsed and Refractory Multiple Myeloma. N Engl J Med *384*, 705-716. https://doi.org/10.1056/NEJMoa2024850.
34. Moreau, P., Garfall, A.L., van de Donk, N., Nahi, H., San-Miguel, J.F., Oriol, A., . . . Usmani, S.Z. (2022). Teclistamab in Relapsed or Refractory Multiple Myeloma. N Engl J Med *387*, 495-505. https://doi.org/10.1056/NEJMoa2203478.
35. Chari, A., Minnema, M.C., Berdeja, J.G., Oriol, A., van de Donk, N., Rodriguez-Otero, P., . . . Krishnan, A. (2022). Talquetamab, a T-Cell-Redirecting GPRC5D Bispecific Antibody for Multiple Myeloma. N Engl J Med *387*, 2232-2244. https://doi.org/10.1056/NEJMoa2204591.
36. Samur, M.K., Fulciniti, M., Aktas Samur, A., Bazarbachi, A.H., Tai, Y.T., Prabhala, R., . . . Munshi, N.C. (2021). Biallelic loss of BCMA as a resistance mechanism to CAR T cell therapy in a patient with multiple myeloma. Nat Commun *12*, 868. https://doi.org/10.1038/s41467-021-21177-5.
37. Da Via, M.C., Dietrich, O., Truger, M., Arampatzi, P., Duell, J., Heidemeier, A., . . . Rasche, L. (2021). Homozygous BCMA gene deletion in response to anti-BCMA CAR T cells in a patient with multiple myeloma. Nat Med *27*, 616-619. https://doi.org/10.1038/s41591-021-01245-5.

38. Swan, D., Madduri, D., and Hocking, J. (2024). CAR-T cell therapy in Multiple Myeloma: current status and future challenges. Blood Cancer J *14*, 206. https://doi.org/10.1038/s41408-024-01191-8.
39. Di Meo, F., Albano, F., Cesarano, A., Wang, Y., Kale, B., Shain, K., . . . Perna, F. (2025). Developing SEMA4A-directed CAR T cells to overcome low BCMA antigen density in multiple myeloma. Cancer Cell *43*, 2298-2310 e2296. https://doi.org/10.1016/j.ccell.2025.09.007.
40. Angelos, M.G., Patel, R.P., Ruella, M., and Barta, S.K. (2024). Progress and Pitfalls of Chimeric Antigen Receptor T Cell Immunotherapy against T Cell Malignancies. Transplant Cell Ther *30*, 171-186. https://doi.org/10.1016/j.jtct.2023.10.013.
41. King, B.F. (2023). Rehabilitation of the P2X5 receptor: a re-evaluation of structure and function. Purinergic Signal *19*, 421-439. https://doi.org/10.1007/s11302-022-09903-0.
42. Uhlen, M., Fagerberg, L., Hallstrom, B.M., Lindskog, C., Oksvold, P., Mardinoglu, A., . . . Ponten, F. (2015). Tissue-based map of the human proteome. Science *347*, 1260419. https://doi.org/10.1126/science.1260419.
43. Karlsson, M., Zhang, C., Méar, L., Zhong, W., Digre, A., Katona, B., . . . Lindskog, C. (2021). A single-cell type transcriptomics map of human tissues. Sci Adv *7*. https://doi.org/10.1126/sciadv.abh2169.
44. Pilcher, W.C., Yao, L., Gonzalez-Kozlova, E., Pita-Juarez, Y., Karagkouni, D., Acharya, C.R., . . . Bhasin, M. (2026). A single-cell atlas characterizes dysregulation of the bone marrow immune microenvironment associated with outcomes in multiple myeloma. Nature Cancer. https://doi.org/10.1038/s43018-025-01072-4.
45. Monaco, G., Lee, B., Xu, W., Mustafah, S., Hwang, Y.Y., Carre, C., . . . Larbi, A. (2019). RNA-Seq Signatures Normalized by mRNA Abundance Allow Absolute Deconvolution of Human Immune Cell Types. Cell Rep *26*, 1627-1640 e1627. https://doi.org/10.1016/j.celrep.2019.01.041.
46. Black, K.L., Naqvi, A.S., Asnani, M., Hayer, K.E., Yang, S.Y., Gillespie, E., . . . Thomas-Tikhonenko, A. (2018). Aberrant splicing in B-cell acute lymphoblastic leukemia. Nucleic Acids Res *46*, 11357-11369. https://doi.org/10.1093/nar/gky946.
47. Yang, S.Y., Hayer, K.E., Fazelinia, H., Spruce, L.A., Asnani, M., Black, K.L., . . . Thomas-Tikhonenko, A. (2023). FBXW7beta isoform drives transcriptional activation of the proinflammatory TNF cluster in human pro-B cells. Blood Adv *7*, 1077-1091. https://doi.org/10.1182/bloodadvances.2022007910.
48. Aguet, F., Anand, S., Ardlie, K.G., Gabriel, S., Getz, G.A., Graubert, A., . . . Volpi, S. (2020). The GTEx Consortium atlas of genetic regulatory effects across human tissues. Science *369*, 1318-1330. https://doi.org/10.1126/science.aaz1776.
49. Goldman, M.J., Craft, B., Hastie, M., Repecka, K., McDade, F., Kamath, A., . . . Haussler, D. (2020). Visualizing and interpreting cancer genomics data via the Xena platform. Nat Biotechnol *38*, 675-678. https://doi.org/10.1038/s41587-020-0546-8.
50. Krause, C., Suwada, K., Blomme, E.A.G., Kowalkowski, K., Liguori, M.J., Mahalingaiah, P.K., . . . Van Vleet, T.R. (2022). Preclinical species gene expression database: Development and meta-analysis. Front Genet *13*, 1078050. https://doi.org/10.3389/fgene.2022.1078050.
51. Polonen, P., Mehtonen, J., Lin, J., Liuksiala, T., Hayrynen, S., Teppo, S., . . . Heinaniemi, M. (2019). Hemap: An Interactive Online Resource for Characterizing Molecular Phenotypes across Hematologic Malignancies. Cancer Res *79*, 2466-2479. https://doi.org/10.1158/0008-5472.CAN-18-2970.
52. Kent, W.J., Sugnet, C.W., Furey, T.S., Roskin, K.M., Pringle, T.H., Zahler, A.M., and Haussler, D. (2002). The human genome browser at UCSC. Genome Res *12*, 996-1006. https://doi.org/10.1101/gr.229102.
53. Ghandi, M., Huang, F.W., Jane-Valbuena, J., Kryukov, G.V., Lo, C.C., McDonald, E.R., 3rd, . . . Sellers, W.R. (2019). Next-generation characterization of the Cancer Cell Line Encyclopedia. Nature *569*, 503-508. https://doi.org/10.1038/s41586-019-1186-3.
54. Schulz, L., Torres-Diz, M., Cortes-Lopez, M., Hayer, K.E., Asnani, M., Tasian, S.K., . . . Thomas-Tikhonenko, A. (2021). Direct long-read RNA sequencing identifies a subset of questionable exitrons likely arising from reverse transcription artifacts. Genome Biol *22*, 190. https://doi.org/10.1186/s13059-021-02411-1.
55. Kotnis, S., Bingham, B., Vasilyev, D.V., Miller, S.W., Bai, Y., Yeola, S., . . . Whiteside, G.T. (2010). Genetic and functional analysis of human P2X5 reveals a distinct pattern of exon 10 polymorphism with predominant expression of the nonfunctional receptor isoform. Mol Pharmacol *77*, 953-960. https://doi.org/10.1124/mol.110.063636.
56. Ongen, H., Buil, A., Brown, A.A., Dermitzakis, E.T., and Delaneau, O. (2016). Fast and efficient QTL mapper for thousands of molecular phenotypes. Bioinformatics *32*, 1479-1485. https://doi.org/10.1093/bioinformatics/btv722.
57. Keats, J.J., Craig, D.W., Liang, W., Venkata, Y., Kurdoglu, A., Aldrich, J., . . . Lonial, S. (2013). Interim Analysis Of The Mmrf Commpass Trial, a Longitudinal Study In Multiple Myeloma Relating Clinical Outcomes To Genomic and Immunophenotypic Profiles. Blood *122*, 532-532. https://doi.org/10.1182/blood.V122.21.532.532.
58. Kaymaz, Y., Oduor, C.I., Yu, H., Otieno, J.A., Ong'echa, J.M., Moormann, A.M., and Bailey, J.A. (2017). Comprehensive Transcriptome and Mutational Profiling of Endemic Burkitt Lymphoma Reveals EBV Type-Specific Differences. Mol Cancer Res *15*, 563-576. https://doi.org/10.1158/1541-7786.MCR-16-0305.

59. Abate, F., Ambrosio, M.R., Mundo, L., Laginestra, M.A., Fuligni, F., Rossi, M., . . . Rabadan, R. (2015). Distinct Viral and Mutational Spectrum of Endemic Burkitt Lymphoma. PLoS Pathog *11*, e1005158. https://doi.org/10.1371/journal.ppat.1005158.
60. Lombardo, K.A., Coffey, D.G., Morales, A.J., Carlson, C.S., Towlerton, A.M.H., Gerdts, S.E., . . . Warren, E.H. (2017). High-throughput sequencing of the B-cell receptor in African Burkitt lymphoma reveals clues to pathogenesis. Blood Adv *1*, 535-544. https://doi.org/10.1182/bloodadvances.2016000794.
61. Bargou, R., Leo, E., Zugmaier, G., Klinger, M., Goebeler, M., Knop, S., . . . Kufer, P. (2008). Tumor regression in cancer patients by very low doses of a T cell-engaging antibody. Science *321*, 974-977. https://doi.org/10.1126/science.1158545.
62. Porazzi, P., Nason, S., Yang, Z., Carturan, A., Ghilardi, G., Guruprasad, P., . . . Ruella, M. (2025). EZH1/EZH2 inhibition enhances adoptive T cell immunotherapy against multiple cancer models. Cancer Cell *43*, 537-551 e537. https://doi.org/10.1016/j.ccell.2025.01.013.
63. Alexandrov, L.B., Nik-Zainal, S., Wedge, D.C., Aparicio, S.A., Behjati, S., Biankin, A.V., . . . Stratton, M.R. (2013). Signatures of mutational processes in human cancer. Nature *500*, 415-421. https://doi.org/10.1038/nature12477.
64. Ruella, M., Korell, F., Porazzi, P., and Maus, M.V. (2023). Mechanisms of resistance to chimeric antigen receptor-T cells in haematological malignancies. Nature Reviews Drug Discovery *22*, 976-995. https://doi.org/10.1038/s41573-023-00807-1.
65. June, C.H., O'Connor, R.S., Kawalekar, O.U., Ghassemi, S., and Milone, M.C. (2018). CAR T cell immunotherapy for human cancer. Science *359*, 1361-1365. https://doi.org/10.1126/science.aar6711.
66. Kahles, A., Lehmann, K.V., Toussaint, N.C., Huser, M., Stark, S.G., Sachsenberg, T., . . . Ratsch, G. (2018). Comprehensive Analysis of Alternative Splicing Across Tumors from 8,705 Patients. Cancer Cell *34*, 211-224 e216. https://doi.org/10.1016/j.ccell.2018.07.001.
67. Pan, Y., Kadash-Edmondson, K.E., Wang, R., Phillips, J., Liu, S., Ribas, A., . . . Xing, Y. (2021). RNA Dysregulation: An Expanding Source of Cancer Immunotherapy Targets. Trends Pharmacol Sci *42*, 268-282. https://doi.org/10.1016/j.tips.2021.01.006.
68. Anczukow, O., Allain, F.H., Angarola, B.L., Black, D.L., Brooks, A.N., Cheng, C., . . . Thomas-Tikhonenko, A. (2024). Steering research on mRNA splicing in cancer towards clinical translation. Nat Rev Cancer *24*, 887-905. https://doi.org/10.1038/s41568-024-00750-2.
69. Torres-Diz, M., Reglero, C., Falkenstein, C.D., Castro, A., Hayer, K.E., Radens, C.M., . . . Thomas-Tikhonenko, A. (2024). An Alternatively Spliced Gain-of-Function NT5C2 Isoform Contributes to Chemoresistance in Acute Lymphoblastic Leukemia. Cancer Res *84*, 3327-3336. https://doi.org/10.1158/0008-5472.CAN-23-3804.
70. Duckwitz, W., Hausmann, R., Aschrafi, A., and Schmalzing, G. (2006). P2X5 subunit assembly requires scaffolding by the second transmembrane domain and a conserved aspartate. J Biol Chem *281*, 39561-39572. https://doi.org/10.1074/jbc.M606113200.
71. de Rijke, B., van Horssen-Zoetbrood, A., Beekman, J.M., Otterud, B., Maas, F., Woestenenk, R., . . . Dolstra, H. (2005). A frameshift polymorphism in P2X5 elicits an allogeneic cytotoxic T lymphocyte response associated with remission of chronic myeloid leukemia. J Clin Invest *115*, 3506-3516. https://doi.org/10.1172/JCI24832.
72. Overes, I.M., de Rijke, B., van Horssen-Zoetbrood, A., Fredrix, H., de Graaf, A.O., Jansen, J.H., . . . Dolstra, H. (2008). Expression of P2X5 in lymphoid malignancies results in LRH-1-specific cytotoxic T-cell-mediated lysis. Br J Haematol *141*, 799-807. https://doi.org/10.1111/j.1365-2141.2008.07125.x.
73. Overes, I.M., Levenga, T.H., Vos, J.C., van Horssen-Zoetbrood, A., van der Voort, R., De Mulder, P.H., . . . Dolstra, H. (2009). Aberrant expression of the hematopoietic-restricted minor histocompatibility antigen LRH-1 on solid tumors results in efficient cytotoxic T cell-mediated lysis. Cancer Immunol Immunother *58*, 429-439. https://doi.org/10.1007/s00262-008-0569-3.
74. Guo, W., Xu, X., Gao, X., Burnstock, G., He, C., and Xiang, Z. (2008). Expression of P2X5 receptors in the mouse CNS. Neuroscience *156*, 673-692. https://doi.org/10.1016/j.neuroscience.2008.07.062.
75. Kim, H., Walsh, M.C., Takegahara, N., Middleton, S.A., Shin, H.I., Kim, J., and Choi, Y. (2017). The purinergic receptor P2X5 regulates inflammasome activity and hyper-multinucleation of murine osteoclasts. Sci Rep *7*, 196. https://doi.org/10.1038/s41598-017-00139-2.
76. Razzoli, M., McGonigle, S., Sahu, B.S., Rodriguez, P., Svedberg, D., Rao, L., . . . Bartolomucci, A. (2024). A key role for P2RX5 in brown adipocyte differentiation and energy homeostasis. Adipocyte *13*, 2421745. https://doi.org/10.1080/21623945.2024.2421745.
77. Abramowski, P., Ogrodowczyk, C., Martin, R., and Pongs, O. (2014). A truncation variant of the cation channel P2RX5 is upregulated during T cell activation. PLoS One *9*, e104692. https://doi.org/10.1371/journal.pone.0104692.
78. Oh, B.L.Z., Shimasaki, N., Coustan-Smith, E., Chan, E., Poon, L., Lee, S.H.R., . . . Campana, D. (2024). Fratricide-resistant CD7-CAR T cells in T-ALL. Nat Med *30*, 3687-3696. https://doi.org/10.1038/s41591-024-03228-8.

79. Patel, R.P., Ghilardi, G., Zhang, Y., Chiang, Y.H., Xie, W., Guruprasad, P., . . . Ruella, M. (2024). CD5 deletion enhances the antitumor activity of adoptive T cell therapies. Sci Immunol *9*, eadn6509. https://doi.org/10.1126/sciimmunol.adn6509.
80. Ruella, M. (2024). CAR-T Therapy for All: Addressing the Access Gap. Transplant Cell Ther *30*, 644-645. https://doi.org/10.1016/j.jtct.2024.06.011.
81. Bhutani, M., Blue, B.J., Cole, C., Badros, A.Z., Usmani, S.Z., Nooka, A.K., . . . Mikhael, J. (2023). Addressing the disparities: the approach to the African American patient with multiple myeloma. Blood Cancer J *13*, 189. https://doi.org/10.1038/s41408-023-00961-0.
82. Paruzzo, L., Eshaghi, K., Ghilardi, G., Doucette, A., Ho, M., Carturan, A., . . . Ruella, M. (2025). Access and outcomes of racial and ethnic minority populations receiving commercial anti-BCMA CART for myeloma. Blood Immunology & Cellular Therapy *1*, 100007. https://doi.org/10.1016/j.bict.2025.100007.
83. Giaquinto, A.N., Miller, K.D., Tossas, K.Y., Winn, R.A., Jemal, A., and Siegel, R.L. (2022). Cancer statistics for African American/Black People 2022. CA Cancer J Clin *72*, 202-229. https://doi.org/10.3322/caac.21718.
84. Kanapuru, B., Fernandes, L.L., Fashoyin-Aje, L.A., Baines, A.C., Bhatnagar, V., Ershler, R., . . . Gormley, N. (2022). Analysis of racial and ethnic disparities in multiple myeloma US FDA drug approval trials. Blood Adv *6*, 1684-1691. https://doi.org/10.1182/bloodadvances.2021005482.
85. Dong, J., Garacci, Z., Buradagunta, C.S., D'Souza, A., Mohan, M., Cunningham, A., . . . Hari, P. (2022). Black patients with multiple myeloma have better survival than white patients when treated equally: a matched cohort study. Blood Cancer J *12*, 34. https://doi.org/10.1038/s41408-022-00633-5.
86. Shenoy, P.J., Malik, N., Sinha, R., Nooka, A., Nastoupil, L.J., Smith, M., and Flowers, C.R. (2011). Racial differences in the presentation and outcomes of chronic lymphocytic leukemia and variants in the United States. Clin Lymphoma Myeloma Leuk *11*, 498-506. https://doi.org/10.1016/j.clml.2011.07.002.
87. Falchi, L., Keating, M.J., Wang, X., Coombs, C.C., Lanasa, M.C., Strom, S., . . . Ferrajoli, A. (2013). Clinical characteristics, response to therapy, and survival of African American patients diagnosed with chronic lymphocytic leukemia: joint experience of the MD Anderson Cancer Center and Duke University Medical Center. Cancer *119*, 3177-3185. https://doi.org/10.1002/cncr.28030.
88. Lee, M.J., Koff, J.L., Switchenko, J.M., Jhaney, C.I., Harkins, R.A., Patel, S.P., . . . Flowers, C.R. (2020). Genome-defined African ancestry is associated with distinct mutations and worse survival in patients with diffuse large B-cell lymphoma. Cancer *126*, 3493-3503. https://doi.org/10.1002/cncr.32866.
89. Pellagatti, A., Armstrong, R.N., Steeples, V., Sharma, E., Repapi, E., Singh, S., . . . Boultwood, J. (2018). Impact of spliceosome mutations on RNA splicing in myelodysplasia: dysregulated genes/pathways and clinical associations. Blood *132*, 1225-1240. https://doi.org/10.1182/blood-2018-04-843771.
90. Vera Alvarez, R., Pongor, L.S., Marino-Ramirez, L., and Landsman, D. (2019). TPMCalculator: one-step software to quantify mRNA abundance of genomic features. Bioinformatics *35*, 1960-1962. https://doi.org/10.1093/bioinformatics/bty896.
91. Sladitschek, H.L., and Neveu, P.A. (2015). MXS-Chaining: A Highly Efficient Cloning Platform for Imaging and Flow Cytometry Approaches in Mammalian Systems. PLoS One *10*, e0124958. https://doi.org/10.1371/journal.pone.0124958.
92. Bustin, S.A., Benes, V., Garson, J.A., Hellemans, J., Huggett, J., Kubista, M., . . . Wittwer, C.T. (2009). The MIQE guidelines: minimum information for publication of quantitative real-time PCR experiments. Clin Chem *55*, 611-622. https://doi.org/10.1373/clinchem.2008.112797.
93. de Jonge, H.J., Fehrmann, R.S., de Bont, E.S., Hofstra, R.M., Gerbens, F., Kamps, W.A., . . . ter Elst, A. (2007). Evidence based selection of housekeeping genes. PLoS One *2*, e898. https://doi.org/10.1371/journal.pone.0000898.
94. Ang, Z., Koean, R.A.G., Er, J.Z., Lee, L.T., Tam, J.K.C., Guo, H., and Ding, J.L. (2019). Novel AU-rich proximal UTR sequences (APS) enhance CXCL8 synthesis upon the induction of rpS6 phosphorylation. PLoS Genet *15*, e1008077. https://doi.org/10.1371/journal.pgen.1008077.

Ang et al, Figure 1

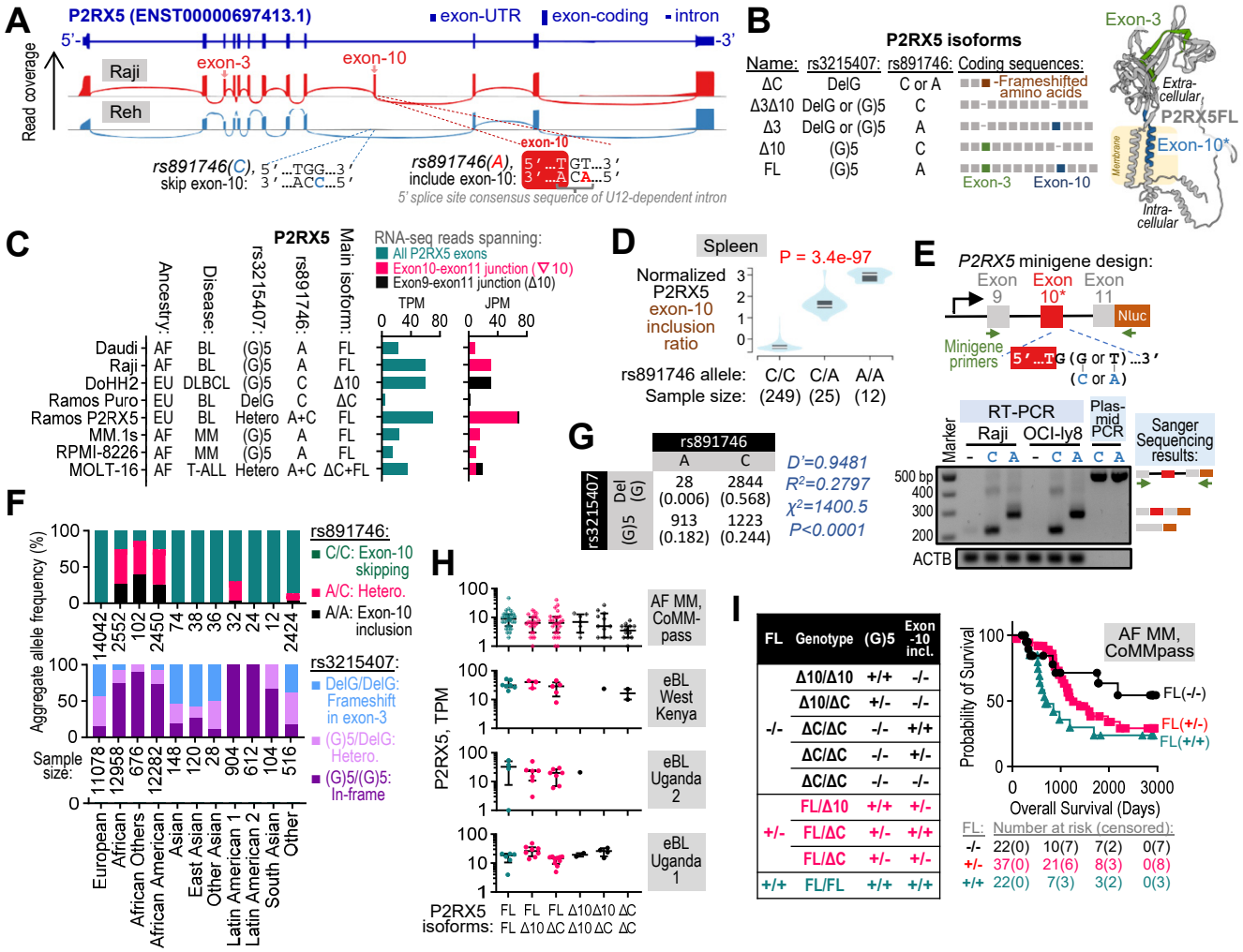

Ang et al, Figure 2

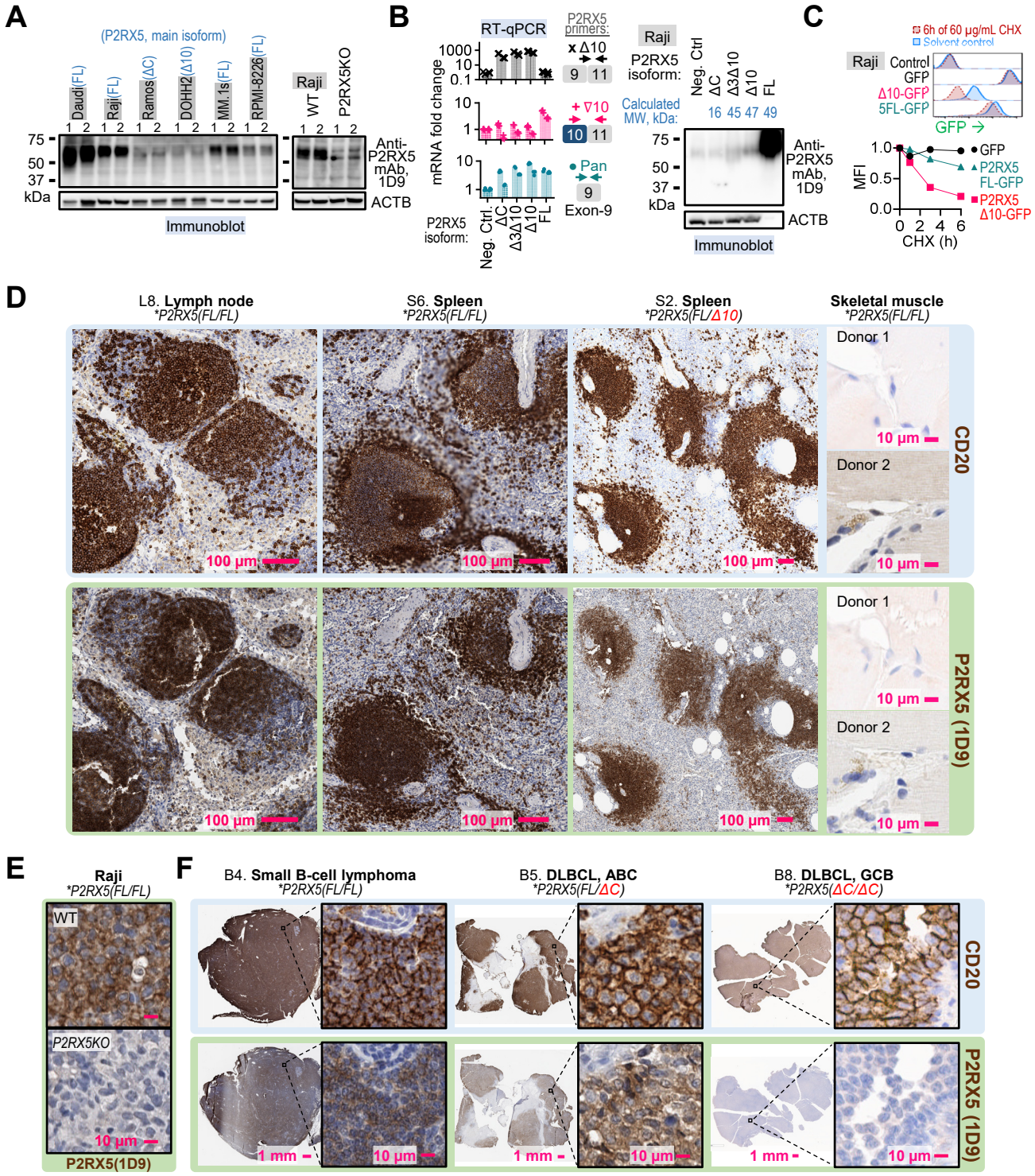

Ang et al, Figure 3

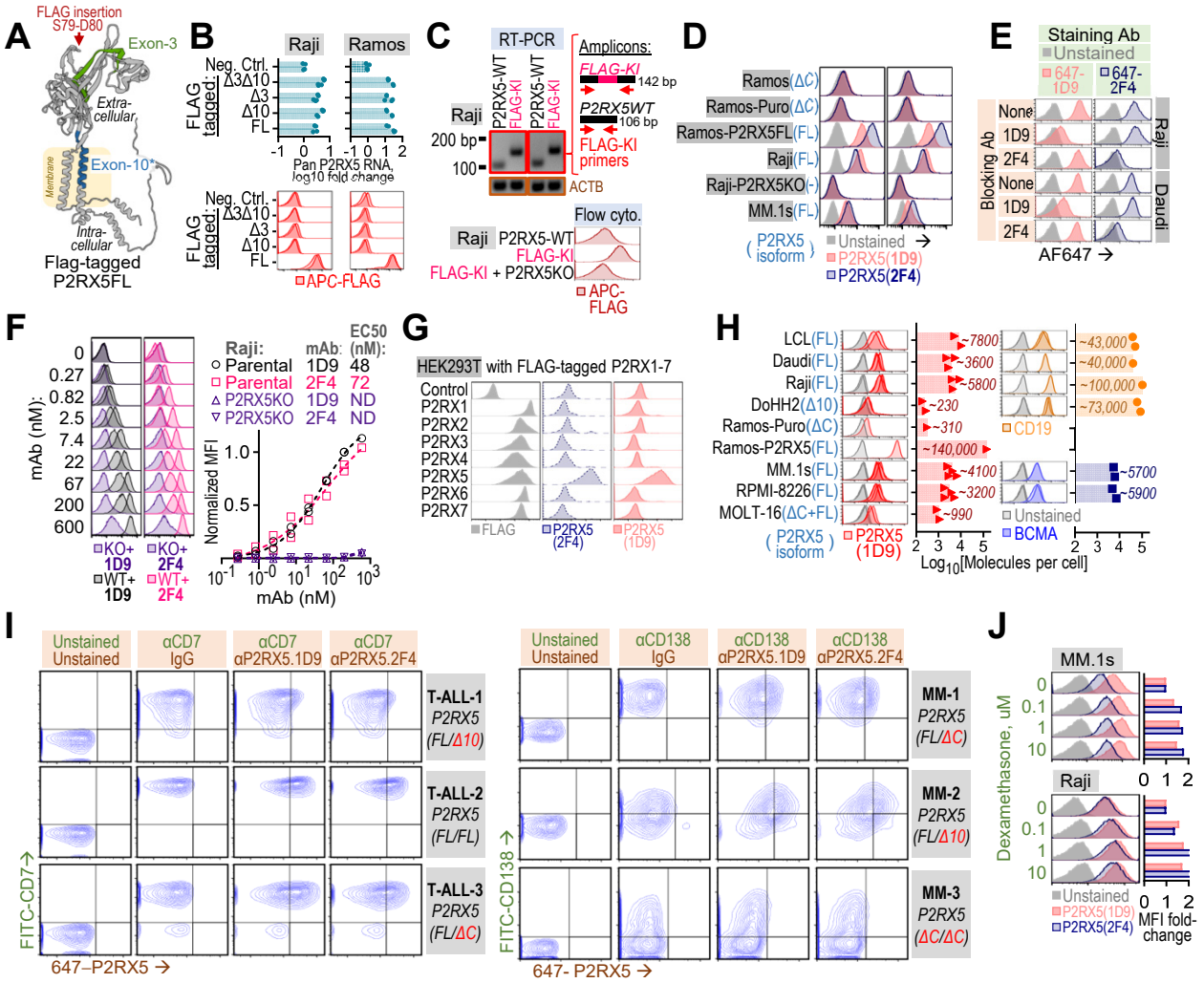

Ang et al, Figure 4

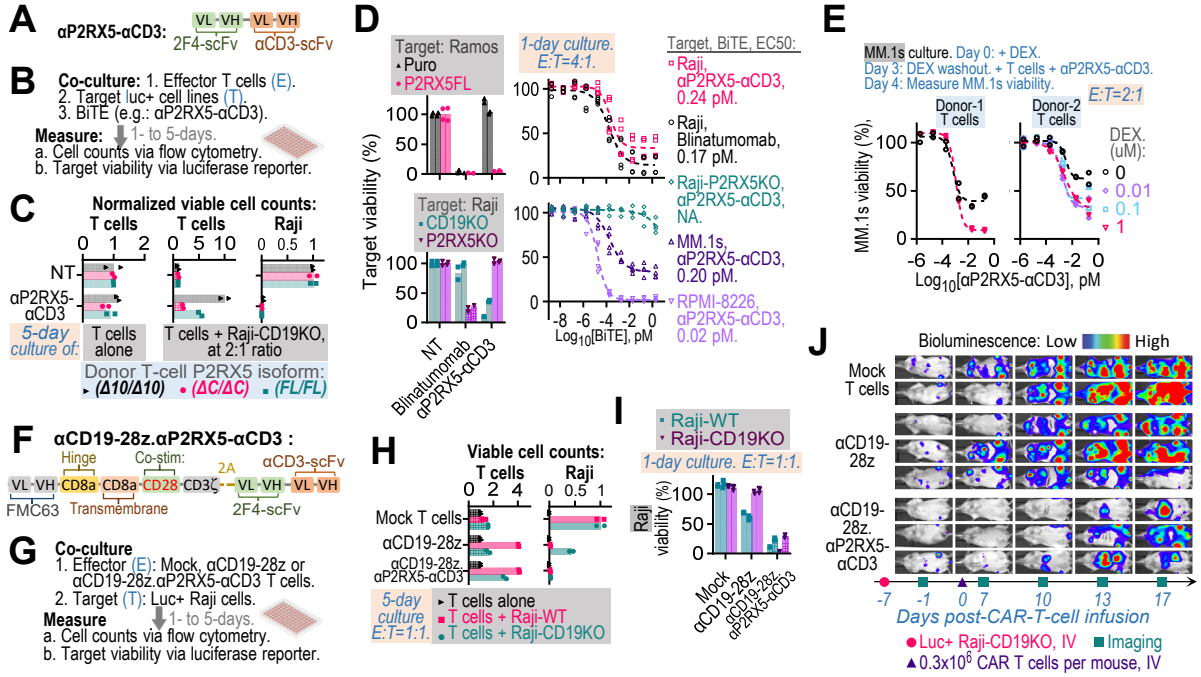

Ang et al, Figure 5

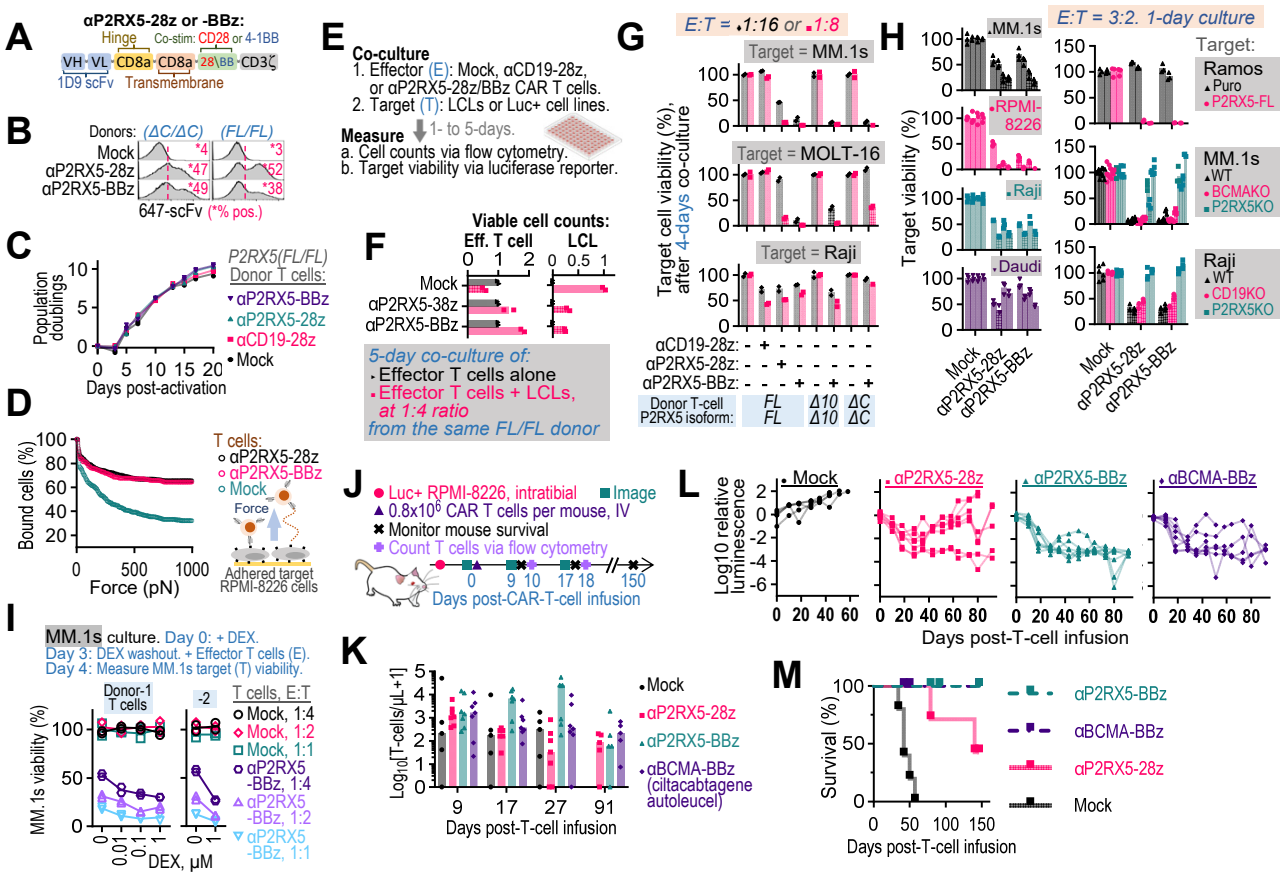

Ang et al, Figure 6